Cellular pharmacodynamics of a novel pyrrolo[3,2-*d*]pyrimidine inhibitor targeting mitochondrial and cytosolic one-carbon metabolism

Aamod S. Dekhne[1], Changwen Ning[4], Md. Junayed Nayeen[2], Khushbu Shah[2], Hasini Kalpage[3], Josephine Frühauf[1], Adrianne Wallace-Povirk[1], Carrie O'Connor[1], Zhanjun Hou[1,5], Seongho Kim[1,5], Maik Hüttemann[3,5], Aleem Gangjee[2], and Larry H. Matherly[1,5,6]

[1]Department of Oncology, Wayne State University School of Medicine / Karmanos Cancer Institute, Detroit, MI 48201

[2]Division of Medicinal Chemistry, Graduate School of Pharmaceutical Sciences, Duquesne University, Pittsburgh, PA 15282

[3]Center for Molecular Medicine and Genetics, Wayne State University School of Medicine, Detroit, MI 48201

[4]Biochemistry and Molecular Biology, Jilin University, Changchun, Jilin Province, China

[5]Molecular Therapeutics Program, Barbara Ann Karmanos Cancer Institute, Detroit, MI 48201

[6]Department of Pharmacology, Wayne State University School of Medicine, Detroit, MI 48201

Running title: Targeting mitochondrial and cytosolic one-carbon metabolism

Corresponding Authors:

Larry H. Matherly, Ph.D., Molecular Therapeutics Program, Barbara Ann Karmanos Cancer Institute, 421 East Canfield Ave, Detroit, MI 48201. Phone: 313-578-4280; fax: 313-578-4287; matherly@karmanos.org

Aleem Gangjee, Ph.D., Division of Medicinal Chemistry, Graduate School of Pharmaceutical Sciences, Duquesne University, 600 Forbes Avenue, Pittsburgh, PA 15282. Phone: 412-396-6070; fax: 412-396-5593; gangjee@duq.edu

Number of Text Pages: 41

Number of Tables: 3

Number of Figures: 7

Number of References: 73

Number of Words in:

    Abstract: 213

    Introduction: 774

    Discussion: 1020

Non-standard abbreviations: 5-aminoimidazole-4-carboxamide, AICA; 5-aminoimidazole-4-carboxamide ribonucleoside, AICAR; carbonyl cyanide-4-(trifluoromethoxy)phenylydrazone, FCCP; 10-formyl tetrahydrofolate synthetase (reverse), MTHFD1L; 5,10-methylene THF dehydrogenase, MTHFD; AMP-activated kinase, AMPK; Chinese hamster ovary, CHO; fetal bovine serum, FBS; folate-free RPMI 1640, FFRPMI; folate receptor, FR; folylpoly-γ-glutamate synthetase, FPGS; reduced glutathione, GSH; glutathione disulfide, GSSG; 2′,7′-dichlorodihydrofluorescein diacetate, H_2DCFDA; human pancreas normal epithelial, HPNE; knockdown, KD; knockout, KO; lactate dehydrogenase, LDH; mammalian target of rapamycin, mTOR; mannose-sucrose, MS; methotrexate, MTX; minimal essential media, MEM; mitochondrial folate transporter, MFT; non-targeted control, NTC; one-carbon, C1; oxygen consumption rate, OCR; phospho-AMPK, P-AMPK; pancreatic cancer, PaC; pemetrexed, PMX; phosphate-buffered saline, PBS; proton-coupled folate transporter, PCFT; resuspension buffer, RSB; reactive oxygen species, ROS; reduced folate carrier, RFC; serine hydroxymethyltransferase, SHMT; succinate dehydrogenase, SDH; tris(2-carboxyethyl)phosphine, TCEP; tetrahydrofolate, THF; wild-type, WT.

Abstract

Folate-dependent one-carbon (C1) metabolism is compartmentalized in the mitochondria and cytosol and is a source of critical metabolites for proliferating tumors. Mitochondrial C1 metabolism including serine hydroxymethyltransferase 2 (SHMT2) generates glycine for *de novo* purine nucleotide and glutathione biosynthesis, and is an important source of NADPH, ATP, and formate, which affords C1 units as 10-formyl-tetrahydrofolate and 5,10-methylene-tetrahydrofolate for nucleotide biosynthesis in the cytosol. We previously discovered novel first-in-class multi-targeted pyrrolo[3,2-*d*]pyrimidine inhibitors of SHMT2 and *de novo* purine biosynthesis at glycinamide ribonucleotide formyltransferase and 5-aminoimidazole-4-carboxamide ribonucleotide formyltransferase with potent *in vitro* and *in vivo* antitumor efficacy toward pancreatic adenocarcinoma cells. In this report, we extend our findings to an expanded panel of pancreatic cancer models. We used our lead analog **AGF347** to characterize pharmacodynamic determinants of antitumor efficacy for this series and demonstrated plasma membrane transport into the cytosol, uptake from cytosol into mitochondria, and metabolism to **AGF347** polyglutamates in both cytosol and mitochondria. Antitumor effects of **AGF347** downstream of SHMT2 and purine biosynthesis included suppression of mTOR signaling, and glutathione depletion with increased levels of reactive oxygen species. Our results provide important insights into the cellular pharmacology of novel pyrrolo[3,2-*d*]pyrimidine inhibitors as antitumor compounds and establish **AGF347** as a unique agent for potential clinical application for pancreatic cancer, as well as other malignancies.

Significance Statement

This study establishes the antitumor efficacies of novel inhibitors of serine hydroxymethyltransferase (SHMT) 2 and of cytosolic targets toward a panel of clinically relevant pancreatic cancer cells and demonstrates the important roles of plasma membrane transport, mitochondrial accumulation, and metabolism to polyglutamates of the compound lead **AGF347** to drug activity. We also establish that loss of serine catabolism and purine biosynthesis resulting from **AGF347** treatment impacts mTOR signaling, glutathione pools and reactive oxygen species, contributing to antitumor efficacy.

Introduction

The malignant phenotype depends on reprogramming cellular metabolism, including the one-carbon (C1) metabolic pathway (Ducker and Rabinowitz, 2017; Hanahan and Weinberg, 2011; Newman and Maddocks, 2017). C1 metabolism is compartmentalized in the cytosol and mitochondria (**Figure 1**) and generates amino acids and nucleotides essential for cell proliferation and tumor progression (Ducker and Rabinowitz, 2017; Tibbetts and Appling, 2010; Yang and Vousden, 2016). C1 pathways depend on tetrahydrofolate (THF) cofactors that mediate transfer of C1 units. In mammalian cells, folates are acquired from exogenous sources and are transported into cells by the reduced folate carrier (RFC) and the proton-coupled folate transporter (PCFT) (**Figure 1**), and by folate receptors (FRs) (not depicted) (Matherly et al., 2007; Zhao, 2011). Once internalized, folates are translocated from the cytosol into mitochondria by the mitochondrial folate transporter (MFT) (SLC25A32) (McCarthy et al., 2004). In both the cytosol and mitochondria, folates are polyglutamylated by folylpoly-γ-glutamate synthetase (FPGS) and these polyglutamyl metabolites do not exchange between compartments (Lawrence et al., 2014). Polyglutamylation of folates confers increased rates of C1 transfer and polyglutamyl folate forms show enhanced cellular retention over monoglutamyl folates (Shane, 1989).

C1 metabolic enzymes in the mitochondria include serine hydroxymethyltransferase 2 (SHMT2), 5,10-methylene THF dehydrogenase 2 (MTHFD2) and 10-formyl THF synthetase (reverse) (MTHFD1L) (**Figure 1**). The serine catabolic pathway is nearly universally activated in cancer, with SHMT2 and MTHFD2 among the most differentially expressed metabolic genes in all human cancers (Jain et al., 2012; Nilsson et al., 2014). The pathway for serine catabolism and glycine synthesis occurs in the mitochondria and the 3-carbon of serine is the major C1 donor for *de novo* biosynthesis of purines and thymidylate in the cytosol (Ducker and Rabinowitz, 2017; Tibbetts and Appling, 2010; Yang and Vousden, 2016). Synthesis of 10-formyl THF from mitochondrial formate and THF in the cytosol stabilizes cytosolic THF from degradation (Zheng et al., 2018). The mitochondrial C1 pathway also generates critical reducing equivalents (as

NAD(P)H) to sustain redox balance in hypoxic tumors (Ye et al., 2014; Zhang et al., 2016a) and is an important source of ATP (Meiser et al., 2016). Genetic deletion of SHMT2 in cultured cells results in defective mitochondrial respiration due to impaired synthesis of respiratory chain proteins (Minton et al., 2018; Morscher et al., 2018), accompanied by increased glycolytic flux (Morscher et al., 2018). Cells deficient in mitochondrial C1 metabolism or MFT transport are glycine auxotrophs (Ducker and Rabinowitz, 2017; Kim et al., 2015; McCarthy et al., 2004; Tibbetts and Appling, 2010).

Evidence of a critical role for serine catabolism as a source of C1 units for cytosolic anabolism (Ducker and Rabinowitz, 2017; Newman and Maddocks, 2017; Yang and Vousden, 2016), combined with the unique demands of tumor cells for glycine and redox balance versus those of normal tissues (Ducker et al., 2016; Jain et al., 2012; Loayza-Puch et al., 2016), suggests that SHMT2 could be an independent prognostic factor and potential therapeutic target for cancer. Elevated SHMT2 is associated with poor prognoses of breast cancers and gliomas (Wang et al., 2017; Wu et al., 2017; Zhang et al., 2016b). In patients who underwent surgical resection of pancreatic adenocarcinomas, elevated SHMT2 was associated with poor overall survival and disease-free survival, compared to patients with low SHMT2 (Noguchi et al., 2018).

We recently described a novel series of 5-substituted pyrrolo[3,2-*d*]pyrimidine compounds (**AGF291**, **AGF320**, and **AGF347**) as anti-cancer agents (Dekhne et al., 2019). Direct inhibition of SHMT2 in mitochondria, and targeting SHMT1 and *de novo* purine biosynthesis (at glycinamide ribonucleotide and 5-aminoimidazole-4-carboxamide (AICA) ribonucleotide formyltransferases; GARFTase and AICARFTase, respectively) in cytosol, was established in colon and lung cancer cells, as well as in pancreatic cancer (PaC) models. For early and late stage MIA PaCa-2 (an aggressive PaC model) tumor xenograft models treated with **AGF347**, impressive *in vivo* antitumor efficacy with curative potential was accompanied by minimal toxicity, and enzyme targets were validated by metabolomics analysis and *in vitro* enzyme assays (Dekhne et al., 2019).

7

In this report, we explore the cellular pharmacodynamics of this series with a focus on **AGF347** (**Figure 2**). Our studies establish broad-spectrum *in vitro* anti-tumor efficacy against a panel of PaC models and demonstrate the critical roles of plasma membrane transport, mitochondrial accumulation, and conversion to polyglutamates in both cytosol and mitochondria in effecting antitumor activity. We also explore mechanisms of anti-tumor activity of pyrrolo[3,2-*d*]pyrimidine compounds including the impact of loss of serine catabolism and purine biosynthesis resulting from **AGF347** (Dekhne et al., 2019) on AMPK activation and mTOR signaling, mitochondrial respiration, and glutathione (GSH) pools and levels of reactive oxygen species (ROS). Collectively, our results underscore the unique pharmacology of this novel series and establish **AGF347** as a promising new therapeutic for cancer.

Materials and Methods

Chemicals. [^{3}H]**AGF347** (9 Ci/mmol), [^{3}H]methotrexate (MTX) (10-30 Ci/mmol) and [^{3}H]folic acid (32.9 Ci/mmol) were purchased from Moravek Biochemicals (Brea, CA). Leucovorin [(6R,S) 5-formyl tetrahydrofolate] and MTX were provided by the Drug Development Branch, National Cancer Institute (Bethesda, MD). Pemetrexed (PMX) was purchased from LC Laboratories (Woburn, MA). Gemcitabine was obtained from Pfizer (New York City, NY). PT523 (N^α-(4-amino-4-deoxypteroyl)-N^δ-hemiphthaloyl-l-ornithine) was a gift of Dr. Andre Rosowsky (Dana-Farber cancer Institute, Boston, MA). Other chemicals were obtained from commercial sources in the highest available purities. **AGF94** (N-((5-[(2-amino-4-oxo-4,7-dihydro-3H-pyrrolo[2,3-*d*]pyrimidin-6-yl)propyl]thiophen-2-yl)carbonyl)-L-glutamic acid), **AGF291** ((4-(3-(2-amino-4-oxo-3,4-dihydro-5*H*-pyrrolo[3,2-*d*]pyrimidin-5-yl)propyl)benzoyl)-L-glutamic acid), **AGF320** ((5-(5-(2-amino-4-oxo-3,4-dihydro-5*H*-pyrrolo[3,2-*d*]pyrimidin-5-yl)pentyl)thiophene-2-carbonyl)-L-glutamic acid), and **AGF347** ((4-(4-(2-amino-4-oxo-3,4-dihydro-5*H*-pyrrolo[3,2-*d*]pyrimidin-5-yl)butyl)-2-

fluorobenzoyl)-L-glutamic acid) were synthesized as previously described (Dekhne et al., 2019; Wang et al., 2011).

Cell culture. The HCT116 cell lines including the SHMT1 and SHMT2 knockout (KO) cells (Ducker et al., 2016; Ducker and Rabinowitz, 2017) were generously provided by G.S. Ducker and J.D. Rabinowitz (Princeton University). KB cells were purchased from ATCC (Manassas, VA) and were cultured as previously described (Deng et al., 2008). PaC cell lines, including AsPC-1 (Chen et al., 1982), BxPC-3 (Tan et al., 1986), CFPAC-1 (Schoumacher et al., 1990), HPAC (Gower et al., 1994), and MIA PaCa-2 (Wu et al., 1977), were generously provided by Dr. Yubin Ge (Karmanos Cancer Institute, Detroit, MI). HPNE (human pancreatic normal epithelial) cells (Lee et al., 2003) were a gift from M. Oulette (University of Nebraska Medical Center, Omaha, NE). Cell lines were validated by STR analysis by Genetica DNA Laboratories (Burlington, NC). MTXRIIOua^{R}2-4 (i.e. R2) Chinese hamster ovary (CHO) cells were provided by Dr. Wayne Flintoff (University of Western Ontario) (Flintoff et al., 1976). From the parental R2 cell line, human RFC and PCFT were individually transfected to generate the isogenic CHO cell lines designated PC43-10 (RFC) and R2/PCFT4 (PCFT) (Deng et al., 2008; Deng et al., 2009; Wong et al., 1995). glyB cells were a generous gift of Dr. Larry Chasin (Columbia University). glyBTII cells were derived from glyB cells by electroporation with human MFT cDNAs in a pcDNA3.1(-)/myc-His6 A-tagged vector. Transfectants were selected with G418, and colonies isolated and expanded for screening by Western blot and real time RT-PCR analyses.

The PaC cell lines were cultured in RPMI 1640 medium, supplemented with 10% fetal bovine serum (FBS) (Sigma-Aldrich, St. Louis, MO), and 1% penicillin/streptomycin (Life Technologies) at 37°C with 5% CO_2. The R1–11 RFC- and PCFT-null HeLa subline was a gift from Dr. I. David Goldman (Albert Einstein School of Medicine, Bronx, NY) (Zhao, 2009). The R1–11-RFC2 cell line was developed in our laboratory by transfection of R1–11 cells with the pZeoSV2-RFC vector and clonal selection (Wang et al., 2015). For non-transport experiments,

9

the above cell lines were maintained in folate-free RPMI 1640 (FFRPMI) supplemented with 10% dialyzed FBS (Sigma-Aldrich, St. Louis, MO), 1% penicillin/streptomycin solution, 2 mM L-glutamine, and 25 nM leucovorin. Cell proliferation assays in CHO cells were performed as described in complete FFRPMI without glycine. Glycine/adenosine rescue experiments were performed in BxPC-3 and HPAC cells without additions, or in the presence of adenosine (60 µM) and/or glycine (130 µM) (Dekhne et al., 2019).

Cell lines were tested for *Mycoplasma* by PCR using a Mycoplasma testing kit (Venor™ GeM Mycoplasma Detection Kit, Sigma) (Feb 2018) and frozen in aliquots in liquid nitrogen. As warranted, cells were treated (Plasmocin, Invivogen) and re-tested for *Mycoplasma*. To avoid cell line "drift", fresh cultures were reconstituted no less than every month from the original freezer stocks (above).

For transport experiments (below), cells were maintained in RPMI 1640 supplemented with 10% FBS, 1% penicillin/streptomycin solution, and 2 mM L-glutamine. R1-11 cells were maintained under continuous selection with 500 µM MTX and 1 mg/ml G418. R1-11 RFC2 cells were maintained under continuous selection with 100 µg/mL Zeocin. CHO cell lines were maintained in α-minimal essential medium (MEM) supplemented with 10% bovine calf serum, 1% penicillin/streptomycin solution, and 2 mM L-glutamine in a humidified atmosphere at 37°C in the presence of 5% CO_2 and 95% air. Additionally, the transfected CHO cell lines (i.e., R2/PCFT4 and glyBTII) were maintained under continuous selection with 1 mg/ml of G418.

Generation of MIA PaCa-2 MFT knockdown (MIA PaCa-2 MFT KD) cell line. MIA PaCa-2 cells were seeded (2 x 10^5 cells/well) in 24 well plates containing 1 ml of culture medium (i.e., FFRPMI supplemented with 10% dialyzed FBS, 1% penicillin/streptomycin, 2 mM L-glutamine, and 25 nM leucovorin). Cells were treated with 4 µg/ml polybrene and 10^5 transducing units of MISSION Lentiviral particles (Sigma-Aldrich) containing shRNA targeting MFT (TRCN0000043091). After 24 h, the medium was replaced with fresh complete FFRPMI medium including 2 µg/ml puromycin

as a selection marker. Once cells were confluent, the cells were harvested, passaged 3-4 times, then assayed by RT-PCR for MFT knockdown relative to non-targeted control (NTC) particle-transduced MIA PaCa-2 cells. To isolate single clones, cells were plated in 100 mm dishes (200 cells/dish) in the presence of 2 µg/ml puromycin. Colonies were isolated, expanded (in RPMI 1640 supplemented with 10% FBS, 1% penicillin/streptomycin, and 2 mM L-glutamine) and clonal cultures were assayed for MFT knockdown via RT-PCR.

Gel electrophoresis and Western blots. glyB and glyBTII cells were cultured in two T150 flasks each and harvested when cells were ~90% confluent. Mitochondrial fractions were isolated (below) and assayed for protein concentrations (Lowry et al., 1951). Equal amounts of protein (36 µg) from each sample were electrophoresed on 10% polyacrylamide gels with SDS (Laemmli, 1970) and transferred to polyvinylidene difluoride membranes (ThermoFisher) (Matsudaira, 1987). To detect MFT (myc-his6) expression, the membranes were incubated for 24 h with rabbit anti-myc primary antibody (MMS-150P; Covance Inc., Princeton, NJ), then with IRDye 800CW-conjugated goat anti-rabbit IgG secondary antibody (925-32211; LICOR Biosciences, Omaha, NE) for 90 min. The blots were scanned with an Odyssey infrared imaging system (LICOR Biosciences). The membrane was prestained with Coomassie Blue as a loading control.

For assays of AMPK and mTOR signaling, total and phospho-AMPK (P-AMPK), and total and phosphorylated S6K1 (P-p70- and P-p80-S6K) were analyzed by Western blotting (Mitchell-Ryan et al., 2013). Briefly, HPAC and BxPC-3 cells (1 million cells/dish for vehicle-treated samples, 1.5 million cells/dish for drug-treated samples) were seeded in 60 mm dishes in 5 ml of FFRPMI supplemented with 10% dialyzed FBS, 1% penicillin/streptomycin, 2 mM L-glutamine, and 25 nM leucovorin. Cells were allowed to adhere for 24 h after which 10 µM **AGF347**, 1 mM AICA ribonucleoside (AICAR), or a comparable volume of vehicle (DMSO) was added. Incubations were performed at 37°C with 5% CO_2. After 48 h, cells were harvested and disrupted by sonication; cell debris was removed by centrifugation (1800 rpm, 5 min, 4°C). The soluble cell

11

fractions were assayed for protein concentration (Lowry et al., 1951) and equal protein (50 µg) from each sample was electrophoresed on 10% polyacrylamide gels with SDS and transferred to polyvinylidene difluoride membranes. To detect phospho- or total AMPK, or p70-S6K1/p85-S6K1, membranes were incubated for 24 h with rabbit primary antibody (total AMPK, 5831S; P-AMPK, T172, 2535S; total p70-S6K1/p85-S6K1, 2708S; P-p70-S6K1/P-p80-S6K1 (T389/T412), 9234S; Cell Signaling Technology, Danvers, MA). The blots were stripped (25 mM glycine pH 2.0, 1-2% SDS) to remove bound antibodies between probing with different antibodies. The blots were developed by incubating in IRDye800CW-conjugated goat anti-rabbit IgG secondary antibody (925-32211; LICOR Biosciences) for 90 min and scanned with an Odyssey infrared imaging system (LICOR Biosciences). Protein loading was normalized to β-actin using anti-β-actin mouse primary antibody (A2228; Sigma-Aldrich St. Louis) and IRDye 800CW-conjugated goat anti-mouse IgG secondary antibody (926-32210; LICOR Biosciences). Densitometry used Image Studio Software (LICOR Biosciences). For densitometry of S6K1, both p70 and p85 bands were quantified. All blots were run at least in duplicate and densitometry data are reported as average values plus/minus ranges.

Real-time PCR. Cells were harvested from either 60 mm dishes or T25 flasks at ~80% confluence and RNAs were extracted using TRIzol reagent (Invitrogen, Carlsbad, CA). cDNAs were synthesized with random hexamers, MuLV reverse transcriptase, and RNase inhibitor (Applied Biosystems, Waltham, MA), and purified with a QIAquick PCR Purification Kit (QIAGEN, Valencia, CA). Quantitative real-time RT-PCR used a Roche LightCycler 480 (Roche Diagnostics, Indianapolis, IN) with gene-specific primers and SYBR Green I dye. Transcript levels were normalized to β-actin and/or glyceraldehyde-3-phosphate dehydrogenase transcripts. Primer sequences are available upon request.

Membrane transport assays. Plasma membrane transport measurements were performed at 37°C as previously described (Ravindra et al., 2018). Buffers used were MES (2-(N-morpholino)ethanesulfonic acid)-buffered saline at pH 5.5 (20 mM MES, 140 mM NaCl, 5 mM KCl, 2 mM $MgCl_2$, and 5 mM glucose), and HEPES (4-(2-hydroxyethyl)-1-piperazineethanesulfonic acid)-buffered saline at pH 6.8 and pH 7.2 (20 mM HEPES, 140 mM NaCl, 5 mM KCl, 2 mM $MgCl_2$, and 5 mM glucose). For some experiments, anion-free buffer at pH 7.2 (20 mM HEPES and 235 mM sucrose) was used. For standard transport experiments, cells were seeded in 60 mm dishes and assayed for uptake when cells were 75-90% confluent with 0.5 µM [^{3}H]MTX or [^{3}H]**AGF347** at 37°C over 2 to 5 min. For the PaC cell lines, uptake was measured at pH 5.5, 6.8, and 7.2 using MES- (pH 5.5) and HEPES- (pH 6.8 and 7.2) buffered saline. Uptake assays in the presence of excess (10 µM) non-radioactive **AGF94** (Wang et al., 2011) (blocks PCFT uptake) and/or PT523 (Rosowsky, 1999) (blocks RFC uptake) were performed to establish transport specificities. Calculations of K_m and V_{max} were performed with concentrations of [^{3}H]**AGF347** or [^{3}H]MTX from 20 to 500 nM for R2/PCFT4 cells (at pH 5.5 in MES-buffered saline) or from 250 nM to 5 µM for R1-11 RFC2 cells (at pH 7.2 in anion-free buffer). K_m and V_{max} values were calculated by Lineweaver-Burk plots. K_i values for each of the drugs relative to 0.5 µM [^{3}H]MTX were calculated from Dixon plots using concentrations of cold competitor (e.g., **AGF347**) from 0 to 500 nM (R2/PCFT4 at pH 5.5 in MES-buffered saline) or 0 to 1 µM (R1-11 RFC2 at pH 7.2 in anion-free buffer).

Subcellular fractionation assays of cytosolic and mitochondrial AGF347. Cells were cultured in complete αMEM supplemented with 10% bovine calf serum (Fisher), 1% penicillin/streptomycin, and 2 mM L-glutamine (glyB and glyBTII CHO cell lines) or complete RPMI 1640 supplemented with 10% FBS, 1% penicillin/streptomycin, and 2 mM L-glutamine (MIA PaCa-2 NTC, MIA PaCa-2 MFT KD, and HPAC). Prior to incubating with radiolabeled compounds, cells were cultured in complete FFRPMI for 48 h. Two T150 flasks per treatment

condition were seeded with 6 (CHO) or 8 (MIA PaCa-2/HPAC) million cells in FFRPMI media supplemented with 60 µM adenosine and 10 µM thymidine (30 mL per T150 flask). Unlabeled MTX or **AGF347** (2 µM, final) and 9 µCi of either [³H]MTX or [³H]**AGF347**, as appropriate, were added. For [³H]folic acid incubations, folate-depleted cells were seeded in complete αMEM or complete RPMI 1640 medium (containing 2.26 µM folic acid) to which 9 µCi of [³H]folic acid was added. Cells were incubated with radiolabel for 48 h; the cytosolic and mitochondrial fractions were separated by differential centrifugation (Clayton and Shadel, 2014). Briefly, cells were trypsinized, washed once with Dulbecco's phosphate-buffered saline (PBS), and resuspended in hypotonic resuspension buffer (RSB; 10 mM NaCl, 1.5 mg MgCl$_2$, 10 mM Tris (pH 7.5)) containing cOmplete Protease Inhibitor Cocktail (Sigma) for 15 min. Cells were lysed with 15 strokes of a B (i.e. "tight-fitting") pestle in a 7 mL Dounce homogenizer. A 2.5x mannitol-sucrose buffer (MS; 5.5 mM mannitol, 175 mM sucrose, 12.5 mM Tris (pH 7.5), 2.5 mM EDTA) containing cOmplete Protease Inhibitor Cocktail (Sigma) was added to a final concentration of 1x MS and an aliquot (i.e., "total" fraction containing both cytosol and mitochondria) was sampled for radioactivity measurement and protein assay (Lowry et al., 1951). The homogenized cell suspension was centrifuged (3100 rpm, 5 min) at 4°C in a Jouan CR4i centrifuge to pellet nuclei and unbroken cells. After collecting the supernatant (contains mitochondria), nuclei and the unbroken cell pellets were resuspended in 1x MS, homogenized with 5 additional strokes, and centrifuged at 3100 rpm. The supernatant was pooled with the previous supernatant and centrifuged at 11,900 rpm at 4°C for 15 min in a Sorvall SS34 rotor to collect the mitochondria. The supernatant (i.e., cytosol fraction) was collected and aliquots were assayed for radioactivity and protein. The mitochondrial pellet was washed once with 1x MS, centrifuged at 11,900 rpm for 15 min, and solubilized in 0.5 N NaOH, after which aliquots were assayed for radioactivity and proteins (i.e., mitochondrial fraction). To assess purities and yields of the cytosolic and mitochondrial fractions, parallel incubations were performed with no inhibitor or radiolabel, and cells were harvested for mitochondria and cytosol fractionation, as described above, and assays of lactate dehydrogenase

14

(LDH) (cytosolic marker) and succinate dehydrogenase (SDH) (mitochondrial marker). LDH was assayed (Royer et al., 1977) in sodium phosphate buffer (0.03 M, pH 7.4) with excess of sodium pyruvate (300 µM) and NADH (70 µM) by measuring the rate of decrease in absorbance at 340 nm. SDH was assayed (Kolaj-Robin et al., 2011) in potassium phosphate buffer (10 mM, pH 7.5 with 1 mM potassium cyanide) with excess sodium succinate (20 mM) and 2,6-dichlorophenolindophenol by measuring the rate of decrease in absorbance at 600 nm.

Measurements of AGF347 polyglutamylation. Synthesis of **AGF347** polyglutamates was assayed in the cytosolic and mitochondrial fractions (above) from MIA PaCa-2 NTC cells, as described (Kugel Desmoulin et al., 2011) with modifications. Briefly, the above protocol for subcellular fractionation was modified by addition of 18 µCi of [³H]**AGF347** to each T150 flask (final concentration 2 µM). Following incubation (48 h), the cytosolic and mitochondrial fractions were isolated, then boiled (10 min), cooled (4°C) and centrifuged (14,000 rpm) in a microcentifuge (4°C for 15 min). The supernatant was fractionated on an Agilent Infinity II 1260 HPLC (Agilent Technologies Inc., Woburn, MA) using a Waters 4 µm Nova-Pak C18 column (3.9 mm × 150 mm) with a Nova-Pak 4 µm C18 guard column (Waters Corporation, Milford, MA). A mobile phase of 100 mM sodium acetate, pH 5.5 (mobile phase A), and 100% acetonitrile (mobile phase B) was used; the gradient was 100% A from 0 to 5 min, followed by a linear increase from 100% A at 5 min to 75%A/25%B at 35 min. The flow rate was 1.6 ml/min. Fractions were collected every minute for the first 5 min, every 30 sec for the next 5 min, and every 10 sec thereafter. Radioactivity was measured with a scintillation counter and the amounts of the individual polyglutamates were calculated from the percentage of total radioactivity in each peak and total picomoles/mg of [³H]**AGF347** in each compartment (mitochondria and cytosol). To confirm the identities of the peaks as **AGF347** polyglutamates, the MIA PaCa-2 cytosolic sample was treated overnight with a preparation of chicken pancreas conjugase (Matherly et al., 1985) in 0.5 ml of 0.1 M sodium borate, pH 7.8, containing 10 mM 2-mercaptoethanol at 32°C to hydrolyze all polyglutamates to

15

the **AGF347** monoglutamyl form. Samples were deproteinized by boiling (5 min) then reanalyzed by HPLC.

Determination of oxygen consumption rate. Oxygen consumption rate (OCR) measurements were made using a Seahorse XFe24 extracellular flux analyzer (Agilent Technologies, Woburn, MA). HCT116 wild-type (WT) and SHMT2 KO cells were grown in complete folate-free, glycine-replete RPMI 1640 supplemented with 10% dialyzed FBS, 1% penicillin/streptomycin, 25 nM leucovorin, 2 mM L-glutamine, and adenosine (60 µM) and treated with **AGF347** (10 µM) or vehicle (DMSO) for 48 h. Cells were then seeded into gelatin-coated XFe24 cell culture microplates in the same media (containing drug) at a density of 130,000 cells per well (5 replicate wells per condition) and allowed to adhere for 24 h. OCRs were monitored at baseline and throughout sequential injections of oligomycin (1 µM), carbonyl cyanide-4-(trifluoromethoxy)phenylhydrazone (FCCP) (1 µM) and rotenone/antimycin A (1 µM each). OCRs were normalized to cell numbers in each well by solubilizing cells with 0.5 N NaOH and assaying proteins by the Folin-phenol method (Lowry et al., 1951).

Measurements of GSH and reactive oxygen species (ROS). HCT116 (WT, SHMT1 KO, and SHMT2 KO), HPAC, and BxPC-3 cells (25,000 cells per well in a 96 well plate), and MIA PaCa-2 cells (40,000 cells per well) were seeded for the ROS assays. For the GSH assays, 20,000 cells per well were seeded. Cells were incubated (24 h) in complete FFRPMI supplemented with 10% dialyzed FBS, 1% penicillin/streptomycin, 25 nM leucovorin, and 2 mM L-glutamine overnight under normoxic conditions (21% O_2, 5% CO_2), at which time the media was replaced with FFRPMI without glycine, supplemented with 10% dialyzed FBS, 1% penicillin/streptomycin, 2 mM L-glutamine, 25 nM leucovorin, and adenosine (60 µM). The cells were treated with 10 µM **AGF347** or an equivalent volume of vehicle (i.e. DMSO) for 24 h under hypoxia (0.5% O_2, 5% CO_2) (Ye et al., 2014); for the ROS assays, parallel incubations (24 h) were also performed in normoxic

16

conditions (21% O_2, 5% CO_2). Cells were then processed for ROS measurements (Biovision, Milpitas, CA; Catalog #: K936) by the 2′,7′-dichlorodihydrofluorescein diacetate (H_2DCFDA) assay and for GSH measurements (Promega, Madison, WI; Catalog #: V6911) by a GSH S-transferase-based luminescence assay following the manufacturers' protocols. To measure total GSH pools (both reduced (GSH) and oxidized (GSSG) forms), cells were treated with 500 µM TCEP (tris(2-carboxyethyl)phosphine) to reduce GSSG to GSH just prior to GSH assay. For the ROS assays, a positive control (ROS inducer) was included in the ROS assay kit. For both ROS and GSH/GSSG levels, results were normalized to cell numbers in each well by solubilizing with 0.5 N NaOH and assaying proteins (Lowry et al., 1951). For the GSH/GSSG assays, protein normalization was based on protein concentrations for identically treated plates that were incubated in parallel with the experimental plate.

Statistics. Sample sizes were predetermined before each experiment. All statistical comparisons were performed using a two-tailed unpaired t-test corrected for unequal variance after data were transformed to meet normality assumptions and no p-value adjustments were made for multiple comparisons. A $\log_{10}$ transformation was used for data with positive values and, when data included zero values, a square root transformation was instead used. For depicting data in plots, all data were summarized with mean values and standard deviations using data without transformation. Geometric mean values and their associated 95% confidence intervals were used to summarize IC_{50} and transport kinetics results using data without transformation in Tables 1 and 2. Experiments that were exploratory in character were descriptively summarized without statistical comparisons.

Results

Demonstration of efficacy and mechanism in a pancreatic cancer cell line panel. Our earlier study (Dekhne et al., 2019) established *in vitro* anti-tumor efficacies of our pyrrolo[3,2-*d*]pyrimidine

17

compounds **AGF291**, **AGF320** and **AGF347** toward H460 lung cancer, HCT116 colon cancer, and MIA PaCa-2 PaC cell line models. With the demonstrated activity of **AGF347** *in vivo* against MIA PaCa-2 PaC xenografts (Dekhne et al., 2019), we extended our studies to include four additional PaC cell lines (HPAC, BxPC-3, CFPAC-1, AsPC-1) characterized by expression of RFC and PCFT, but not FRα (**Figure S1**). Proliferation results with the PaC cell lines were compared to those for HPNE (human pancreatic normal epithelial) cells (Lee et al., 2003). For HPAC, BxPC-3, CFPAC-1, and AsPC-1 cells, the compounds showed increased (~4-9-fold) inhibitory activity relative to MIA PaCa-2 cells (**Table 1**). **AGF347** (**Figure 2**) was consistently the most active of the series, with the lowest IC_{50} values recorded in the HPAC (194 nM) and BxPC-3 (80 nM) cells. In HPNE cells, the pyrrolo[3,2-*d*]pyrimidine analogs were inactive up to 5000 nM (**Table 1**).

To confirm the targeted pathways for **AGF347** in HPAC and BxPC-3 cells, we performed "rescue" experiments in *glycine- and nucleoside-free* media (Dekhne et al., 2019), to assess the protective effects of supplemented glycine (130 μM) and/or adenosine (60 μM) (**Figure 2**). Neither glycine nor adenosine alone rescued cell proliferation from the effects of **AGF347**, although the combination effected complete rescue. These results are entirely consistent with our earlier studies (Dekhne et al., 2019) that established the inhibition of mitochondrial C1 metabolism and *de novo* purine biosynthesis by **AGF347** in MIA PaCa-2 cells.

Determination of plasma membrane transport of AGF347. Previous studies of antiproliferative activities of **AGF291**, **AGF320**, and **AGF347** toward isogenic CHO cells engineered to individually express RFC or PCFT suggested cellular uptake of this series by these facilitative transporters (Dekhne et al., 2019). To directly measure transport of **AGF347** by these systems, we performed transport assays with [³H]**AGF347** in cell lines engineered to individually express RFC (R1-11RFC2 HeLa (Wang et al., 2015)) or PCFT (R2/PCFT4 CHO (Deng et al., 2009)). Transport of [³H]**AGF347** (0.5 μM) was measured over 5 min at pH 7.2 (RFC) or pH 5.5 (PCFT) (approximating the respective pH optima) at 37°C and results were compared to those with [³H]MTX. For both

18

[3H]MTX and [3H]**AGF347**, transport was substantial for both PCFT and RFC. Transport was effectively abolished ($\geq$ 90%) by excess unlabeled substrates with specificity for PCFT (**AGF94** (Wang et al., 2011)) and RFC (**PT523** (Rosowsky, 1999)) (**Figures 3A** and **3B**, respectively). Transport kinetics were determined for [3H]MTX and [3H]**AGF347**. For both PCFT and RFC, the differences in V_{max} values for **AGF347** versus MTX were not significant. The differences in K_m values for MTX versus **AGF347** with RFC were also insignificant, whereas **AGF347** had a significant 5.8-fold decreased K_m for PCFT (0.057 µM vs 0.329 µM, respectively) compared to MTX (**Table 2**).

Transporter binding for the pyrrolo[3,2-*d*]pyrimidine analogs **AGF291**, **AGF320**, and **AGF347** (Dekhne et al., 2019) was further assessed by calculating K_i values by Dixon analysis with [3H]MTX in the PCFT and RFC engineered cell lines, using the calculated K_m and V_{max} values for [3H]MTX. The results were compared to those calculated for **AGF94** and PMX (**Table 2**). By these analyses, K_i values for **AGF291**, **AGF320**, and **AGF347** for RFC were essentially equivalent (range of 0.200 to 0.274 µM) and were 2- to 3-fold lower than that for PMX (0.583 µM). For PCFT, the K_i for **AGF347** (0.070 µM) was 2- to 2.5-fold lower than that for **AGF291** (0.163 µM) and **AGF320** (0.142 µM) and was equivalent to that for **AGF94** (0.070 µM); the K_i for **AGF347** was similar to that for PMX (0.056 µM), among the best PCFT substrates (Unal et al., 2008; Wang et al., 2011).

To extend these transport analyses to the assorted PaC cell lines, we measured uptake of [3H]**AGF347** at both pH 5.5 and pH 7.2 in the presence or absence of excess (10 µM) unlabeled **AGF94** and/or PT523 to gauge the relative contributions of PCFT and RFC, respectively, to [3H]**AGF347** uptake. Our experiments revealed substantial uptake of [3H]**AGF347** by PCFT at pH 5.5 and by RFC at pH 7.2 (**Figures 3C and D**). At pH 5.5, PCFT uptake was blocked by **AGF94**, albeit incompletely (~30-90%); this suggests a contribution from a non-PCFT transporter in addition to PCFT. Analogous results were recorded at pH 7.2, although transport was blocked (~65-85%) by PT523, demonstrating principal involvement of RFC.

19

Experiments with the PaC cell lines were extended to pH 6.8, approximating the pH of the tumor microenvironment (Stubbs et al., 2000). At pH 6.8, (**Figure 3E**) uptake of [³H]**AGF347** was mediated by both PCFT and RFC such that the transport inhibition by both **AGF94** and PT523 together was substantial and ranged from ~70-90%. Uptake of [³H]**AGF347** by RFC predominated at pH 6.8, as reflected in the generally greater decrease in net uptake for samples treated with PT523 compared to those treated with **AGF94**. Collectively, these studies establish important roles for both RFC and PCFT in the uptake of **AGF347** by PaC cells.

Subcellular compartmentation of AGF347 and metabolism to polyglutamates. Implicit to targeting of mitochondrial C1 metabolism by our pyrrolo[3,2-*d*]pyrimidine inhibitors (Dekhne et al., 2019) is their uptake and accumulation in the mitochondria. Further, as these molecules are negatively charged, they likely require facilitated uptake into mitochondria, possibly mediated by the MFT, the only known transporter of folates into the mitochondrial matrix (Lawrence et al., 2011; McCarthy et al., 2004).

We assessed mitochondrial accumulation of [³H]**AGF347** by MIA PaCa-2 cells, in comparison to [³H]folic acid and [³H]MTX. To determine whether MFT contributes to mitochondrial uptake of [³H]**AGF347**, we transfected human MFT (myc-His6-tagged) into MFT-null glyB CHO cells (McCarthy et al., 2004) to generate the glyBTII cell line (**Figure S2A** shows a Western blot of glyB and glyBTII cell extracts probed with Myc antibody confirming ectopic MFT-myc-His6 expression). For MIA PaCa-2 cells, we generated non-targeted control (NTC) and MFT shRNA KD (MFT KD) cells to assess the transport role of MFT in a human tumor model (**Figure S2B)**. We also measured mitochondrial uptake of [³H]**AGF347** and [³H]MTX in HPAC cells.

The cell lines were cultured for 48 h, after which [³H]folic acid (2.26 μM), [³H]MTX (2 μM) or [³H]**AGF347 (**2 μM) were added for an additional 48 h (in the presence of 60 μM adenosine and 10 μM thymidine to abrogate any potential cytotoxic drug effects (Dekhne et al., 2019; Deng et al., 2008)). Mitochondrial and cytosolic fractions were isolated by differential centrifugation

20

(Clayton and Shadel, 2014) with the radioactivity in each fraction quantified (**Figures 4A-C**) and normalized to protein (**Figures 4D-F**). LDH (Lin et al., 1993) and SDH catalytic activities (Munujos et al., 1993) were used as measures of purity and cross-contamination between the cytosolic and mitochondrial fractions, respectively (**Table S1**). While the mitochondrial fractions were highly pure (<5% cytosolic contamination), cytosolic fractions were contaminated with lysed mitochondria.

Substantial uptake of [3H]folic acid and [3H]**AGF347** was detected in both cytosolic and mitochondrial fractions of the glyBTII CHO and MIA PaCa-2 NTC sublines, with the mitochondrial fraction comprising 20-33% of the total accumulated [3H]folic acid and 14-16% of the total [3H]**AGF347** (**Figures 4A-C**) in cells. Cytosolic [3H]MTX accumulations were modest and there were disproportionately low levels of [3H]MTX in mitochondria as reported (Lin et al., 1993). Analogous results were obtained for HPAC cells (**Figure 4B and C**). Thus, [3H]**AGF347** accumulates significantly in the mitochondria.

[3H]Folic acid accumulations significantly decreased in the MIA PaCa-2 MFT KD (~50%) and glyB (MFT-null) (~90%) cell lines compared to their MFT-functional counterparts (**Figure 4F**); this is consistent with MFT-mediated uptake of [3H]folic acid metabolites (McCarthy et al., 2004). Although the mitochondrial accumulation of [3H]**AGF347** was likewise decreased (~35%) in glyB cells, compared to glyBTII cells, this was less than that for [3H]folic acid. Further, there was no difference in the mitochondrial uptake of [3H]**AGF347** between the MIA PaCa-2 NTC and MFT KD sublines. Collectively, these results indicate that mitochondrial accumulation of [3H]**AGF347** is at least partially mediated by MFT.

As FPGS is expressed as cytosolic and mitochondrial-specific isoforms and polyglutamate folate cofactors are detected in both compartments (Lawrence et al., 2014), we assessed whether [3H]**AGF347** polyglutamates could be identified in the cytosolic and mitochondrial fractions. The cytosolic and mitochondrial fractions from MIA PaCa-2 NTC cells incubated with [3H]**AGF347** were fractionated by HPLC for detection of [3H]**AGF347** polyglutamates and unmetabolized

[³H]**AGF347**. In addition to the parent monoglutamyl [³H]**AGF347**, at least six metabolites (PG$_{2-7}$) were resolved in the cytosolic extract (**Figure 4G**), and three metabolites (labeled PG$_{5-7}$ based on the elution times for the cytosolic extract) were detected in the corresponding mitochondrial extract (**Figure 4H**). To confirm identities of the peaks as polyglutamyl metabolites of [³H]**AGF347**, aliquots of the MIA PaCa-2 NTC cytosolic fraction were treated with chicken pancreas conjugase (Kugel Desmoulin et al., 2011). The early-eluting metabolites quantitatively (>95%) reverted to parent [³H]**AGF347** (**Figure 4I**), confirming that these radiolabeled metabolites were polyglutamyl forms of [³H]**AGF347**. These results establish near-complete metabolism to [³H]**AGF347** polyglutamates in both the cytosol and mitochondria of MIA PaCa-2 cells (**Table 3**), suggesting that **AGF347** is an excellent substrate for FPGS in both compartments. In both the cytosol and the mitochondria, the pentaglutamyl and hexaglutamyl predomidated.

Downstream effects of targeting SHMT2 and de novo purine biosynthesis by AGF347. We previously reported that the pyrrolo[3,2-*d]*pyrimidine compounds **AGF291**, **AGF320**, and **AGF347** all targeted SHMT2 in the mitochondria, and SHMT1 and the purine biosynthetic enzymes GARFTase and/or AICARFTase in the cytosol (Dekhne et al., 2019). Inhibition of *de novo* purine biosynthesis was accompanied by elevation of AICA ribonucleotide (ZMP) and suppression of cellular purine nucleotide pools (Dekhne et al., 2019). We considered the possibility that downstream effects of these inhibitions that could significantly contribute to the antitumor efficacy of **AGF347** and related compounds *in vitro* and *in vivo* (Dekhne et al., 2019), including those involving (i) mTOR signaling (Racanelli et al., 2009; Rothbart et al., 2010) (ii) mitochondrial respiration (Minton et al., 2018; Morscher et al., 2018), and (iii) elevated ROS due to decreased glycine synthesis and GSH pools (Ye et al., 2014).

**Inhibition of mTOR signaling.** Both elevated AICA ribonucleotide (via activation of AMP-activated protein kinase (AMPK)) (Racanelli et al., 2009; Rothbart et al., 2010) and decreased

purines (Hoxhaj et al., 2017) can suppress the pro-survival mTOR pathway (Lim et al., 2015). As Ras-ERK exhibits "cross-talk" with AMPK-mTOR signaling (Liang et al., 2018; Mann et al., 2016; Mendoza et al., 2011), we assessed the impact of **AGF347** treatment (10 µM, 48 h) on both BxPC-3 (KRAS WT) and HPAC (KRAS mutant) PaC cell lines by analyzing changes in phosphorylation of AMPK (P-AMPK) and the mTOR effectors p70- and p85-S6K1 (Magnuson et al., 2012) by Western blotting. Treatment with AICAR (1 mM) elevates AICA ribonucleotide levels and was used as a positive control (Mitchell-Ryan et al., 2013). Results are shown in **Figure 5**.

AICAR treatment of both BxPC-3 and HPAC cells induced AMPK hyperphosphorylation (3.87 (+/-0.17) and 1.32 (+/-0.03) fold, respectively) compared to untreated controls. This was accompanied by decreased phospho-S6K1 (p85- and p70-S6K1) in both BxPC-3 (0.16 (+/-0.02) compared to the control value of 1) and HPAC (0.20 (+/-0.01)) cells. **AGF347** induced a modestly increased activation of AMPK in the BxPC-3 cells (1.93 (+/-0.09) fold increased P-AMPK) compared to HPAC cells (1.25 (+/-0.06) fold). In BxPC-3 cells, **AGF347** treatment induced hypo-phosphorylation of S6K1 (0.62 (+/-0.04)) but not HPAC cells (1.01 (+/-0.02)) compared to controls.

These results suggest that AMPK activation and loss of mTOR signaling may contribute to the anti-tumor efficacy of **AGF347**. However, the magnitude of these effects vary in different tumor models and may be muted in KRAS-mutant cells, such as HPAC.

Effects on mitochondrial respiration. As SHMT2 serves a critical role in respiratory chain protein synthesis via methylation of select mitochondrial tRNAs, with SHMT2 KO cells experiencing respiratory deficiencies (Lucas et al., 2018; Minton et al., 2018; Morscher et al., 2018), we examined whether suppression of SHMT2 by **AGF347** resulted in an analogous effect on mitochondrial respiration. For these experiments we used HCT116 WT and HCT116 SHMT2 KO cells (Morscher et al., 2018) from our prior study (Dekhne et al., 2019) to directly compare effects on the OCR resulting from inhibition of SHMT2 by **AGF347** to that resulting from complete KO of SHMT2. HCT116 cells were pretreated with vehicle (DMSO; WT and SHMT2 KO) or 10

23

µM **AGF347** (WT) for 48 h as before (Dekhne et al., 2019). Cells were seeded and the next day were subjected to a mitochondrial stress test (**Figure 6**). As previously reported (Lucas et al., 2018; Minton et al., 2018; Morscher et al., 2018), the SHMT2 KO cells showed a substantially reduced respiratory capacity relative to WT cells. In spite of the confirmed inhibition of SHMT2 (Dekhne et al., 2019), **AGF347** caused no repressive effect on basal respiration, ATP production (H$^+$ leak), maximal respiration or non-mitochondrial respiration compared with WT cells (**Figure 6**).

Impact of AGF347 on reactive oxygen species (ROS) and GSH pools. SHMT2 is critical for synthesis of glycine for generation of reduced glutathione (GSH) (Ducker and Rabinowitz, 2017) and previous work has shown *de novo* GSH biosynthesis is more sensitive to glycine depletion than either *de novo* purine or protein biosynthesis (Ducker et al., 2017). GSH functions to scavenge ROS that are byproducts of oxidative phosphorylation, especially under hypoxic conditions that induce an "electron leak" from the electron transport chain (Chandel et al., 2000; Guzy et al., 2005).

To assess induction of ROS upon treatment with **AGF347** (10 µM), we treated HCT116, BxPC-3, HPAC, and MIA PaCa-2 cells with inhibitor for 24 h under normoxic (21% O$_2$, 5% CO$_2$) and hypoxic (0.5% O$_2$, 5% CO$_2$ (Ye et al., 2014)) conditions. As controls, we included HCT116 SHMT1 KO and SHMT2 KO cells. To prevent rescue of GSH pools by extracellular glycine, we performed these experiments in *glycine-free* media supplemented with adenosine (60 µM) (isolates effects of SHMT2 inhibition from those resulting from *de novo* purine biosynthesis inhibition). Total cellular ROS was measured with a H$_2$DCFDA reporter assay (Eruslanov and Kusmartsev, 2010). Functional induction of cellular hypoxia under 0.5% O$_2$ was reflected in elevated transcripts for carbonic anhydrase IX (**Figure 7A**), an established hypoxia marker (Benej et al., 2014). Under normoxic conditions (**Figure 7B**), treatment with **AGF347** induced no significant accumulation of ROS in any of the cell lines. Conversely, under hypoxia (**Figure 7C**),

24

significant accumulation of ROS occurred in HCT116 WT (~2-fold) and HPAC cells (1.5-fold) treated with **AGF347**, although there was no increased ROS in BxPC-3 and MIA PaCA-2 cells treated with the inhibitor. HCT116 SHMT2 KO cells induced a 3-fold increase in ROS (under hypoxic conditions) whereas there was no significant increase in ROS in SHMT1 KO cells. Thus, complete loss of SHMT2 in HCT116 cells results in increased ROS. Further, the extent of ROS induction with **AGF347** varies with different cell lines. These results suggest that ROS could be an important mediator of **AGF347** anti-tumor effects in hypoxic tumors.

To assess the possibility that decreased GSH due to loss of glycine or redox potential resulting from loss of SHMT2 activity was causal in the increased ROS in certain cell lines, we assayed GSH (reduced GSH + glutathione disulfide (GSSG)) in HCT116, BxPC-3, HPAC, and MIA PaCa-2 cells under hypoxic conditions. Consistent with the changes in ROS, both reduced and total GSH pools were significantly decreased with **AGF347** treatment in HCT116 and HPAC cell lines paralleling changes in ROS (**Figure 7D and 7C**). Although decreases in reduced and total GSH were also detected in MIA PaCa-2 cells, in BxPC-3 cells these were unchanged. Interestingly, HCT116 SHMT2 KO cells showed substantially elevated ROS yet unchanged reduced and total GSH.

Collectively, these results establish that suppression of *de novo* GSH biosynthesis and elevated ROS are potential mechanisms *of in vivo* cytotoxic activity by **AGF347** although this varies with different tumor cells.

Discussion

Although targeting of C1 metabolism for cancer has shown clinical utility from the early days of chemotherapy to the present, the clinical effectiveness of drugs targeting these pathways is limited by their toxicities toward normal tissues. Therefore, agents targeting tumor-selective enzymes, such as those involved in mitochondrial C1 metabolism (Nilsson et al., 2014), would offer immense clinical utility.

In this study, we characterized the cellular pharmacodynamics of **AGF347**, a prototype and lead analog of a novel series of 5-substituted pyrrolo[3,2-*d*]pyrimidine compounds that inhibit mitochondrial C1 metabolism at SHMT2, with downstream inhibitions of cytosolic C1 targets including SHMT1 and the *de novo* purine biosynthetic enzymes GARFTase and AICARFTase (Dekhne et al., 2019). We focused on a series of 5 PaC cell lines (including those with different KRAS mutation status) based on our previous results that established substantial anti-tumor efficacy of **AGF347** toward MIA PaCa-2, an aggressive PaC model with mutant KRAS (Dekhne et al., 2019). Whereas all the analogs were active toward the PaC cell lines over an 11-fold range of growth inhibition, **AGF347** was consistently the most active of the series. Further, tumor selectivity was strongly implied as the pyrrolo[3,2-*d*]pyrimidine inhibitors were inert toward HPNE cells.

We characterized the transport properties for [³H]**AGF347**, including transport kinetics compared to [³H]MTX with both RFC and PCFT, the major transport systems for folates and related compounds in the PaC cell lines. Transport of **AGF347** by both RFC and PCFT was substantial. For the tumor-selective transporter PCFT, **AGF347** showed a binding affinity approaching those of the best PCFT substrates **AGF94** and PMX (Desmoulin et al., 2012) and far exceeding that of MTX. In the PaC cell lines, transport of [³H]**AGF347** by both PCFT and RFC was substantial at pH 6.8 (approximating pH conditions associated with the tumor microenvironment), although transport by RFC predominated.

As the pyrrolo[3,2-*d*]pyrimidine compounds target SHMT2 in the mitochondria (Dekhne et al., 2019), we assessed the mitochondrial accumulation of [³H]**AGF347** in MIA PaCa-2 cells and in MFT-null glyB CHO cells transfected with human MFT. For both cell lines, significant [³H]**AGF347** accumulated in both the cytosol and mitochondria at levels similar to those for [³H]folic acid metabolites and far in excess of [³H]MTX. As MFT is the only known mitochondrial transporter (McCarthy et al., 2004), the decreased mitochondrial accumulation of [³H]**AGF347** in MFT-null glyB cells compared to glyBTII cells transfected with human MFT (albeit less than for

[^{3}H]folic acid), suggested that mitochondrial uptake of **AGF347** must be at least partly mediated by MFT. However, partial (~80%) MFT knockdown in MIA PaCa-2 cells had a nominal impact on mitochondrial accumulation of [^{3}H]**AGF347** in contrast to [^{3}H]folic acid. This suggests that even a small amount of MFT is sufficient to mediate accumulation of **AGF347** in the mitochondria, and/or that an additional mitochondrial transporter must also be involved in **AGF347** uptake. Following uptake, **AGF347** polyglutamates accumulated in the mitochondria which likely contribute to sustained SHMT2 inhibition and *in vivo* antitumor activity of **AGF347** (Dekhne et al., 2019). By analogy with pemetrexed, it is likely that the polyglutamyl derivatives that accumulate in the mitochondria and cytosol contribute to inhibition of cytosolic enzyme targets and are more potent enzyme inhibitors than the K_i values for the monoglutamate form would suggest (Dekhne et al., 2019). By analogy with folate polyglutamates (Lawrence et al., 2014), **AGF347** polyglutamates are unlikely to be MFT substrates and the accumulation of **AGF347** polyglutamates in the cytosol may actually restrict drug accumulation in the mitochondria and SHMT2 inhibition.

We investigated mechanisms that directly or indirectly contribute to the anti-tumor effects of **AGF347** secondary to targeting SHMT2 in mitochondria and *de novo* purine biosynthesis and SHMT1 in the cytosol (Dekhne et al., 2019). These include possible effects on AMPK and mTOR signaling, mitochondrial respiration, and GSH and GSSG levels and ROS scavenging. For BxPC-3 cells with WT KRAS, **AGF347** increased AMPK phosphorylation and suppressed mTOR signaling, suggesting that loss of mTOR signaling plays a role in the anti-tumor efficacy of **AGF347** in these cells. Inhibitor effects on AMPK and S6K1 were muted in KRAS-mutant HPAC cells, suggesting Ras-ERK crosstalk with AMPK-mTOR signaling could interfere with this mechanism (Mendoza et al., 2011). However, additional studies with a wider range of KRAS-WT and KRAS-mutant cells will be necessary to conclusively establish this association. There was no effect of **AGF347** on mitochondrial respiration, in contrast to that resulting from genetic KO of SHMT2 in HCT116 cells. This suggests that the extent of SHMT2 inhibition by **AGF347** is incomplete and likely insufficient to suppress mitochondrial respiration, consistent with the

27

findings of Minton et al. (Minton et al., 2018) who reported that impaired mitochondrial respiration requires complete suppression of SHMT2 activity. **AGF347** effected decreased levels of reduced and total GSH, likely reflecting the principal role of SHMT2 in the synthesis of glycine required for GSH and its impact on redox balance (Ducker and Rabinowitz, 2017). For HCT116 SHMT2 KO cells, reduced and total GSH pools were unchanged, possibly due to a compensatory reversal of the SHMT1 reaction (Ducker et al., 2016) which results in restored glycine synthesis and the preservation of the GSH pools. As this was not seen with cells treated with **AGF347**, this likely reflects the dual inhibition of both SHMT1 and SHMT2 by this compound (Dekhne et al., 2019). Decreased total GSH pools were accompanied by increased ROS (under hypoxic conditions) in some but not all the cell lines, possibly reflecting (in part) reliance on alternate anti-oxidant pathways such as thioredoxin in some cases (Birben et al., 2012).

In conclusion, the results described herein underscore the biological novelty and multifaceted mechanisms-of-action for the 5-substituted pyrrolo[3,2-*d*]pyrimidine compounds typified by **AGF347** and are entirely consistent with its substantial *in vivo* anti-tumor potency and nominal and reversible toxicity (Dekhne et al., 2019). Tumor specificity for this series of compounds is broad and likely reflects a selective reliance on mitochondrial C1 metabolism (Jain et al., 2012; Nilsson et al., 2014) and *de novo* purine biosynthesis over purine salvage (Subhi et al., 2004) in cancer cells, with downstream inhibition of mTOR signaling, decreased GSH pools and increased ROS. This series of compounds affords an exciting new platform for broad-spectrum anticancer drug development.

Authorship Contributions

Participated in research design: Dekhne, Ning, Kalpage, Hou, Hüttemann, Matherly

Conducted experiments: Dekhne, Ning, Kalpage, Frühauf, Wallace-Povirk, O'Connor

Contributed new reagents or analytic tools: Nayeen, Shah, Gangjee

Performed data analysis: Dekhne, Ning, Frühauf, Kim, Matherly

Wrote or contributed to the writing of the manuscript: Dekhne, Hou, Gangjee, Matherly

References

Benej M, Pastorekova S and Pastorek J (2014) Carbonic anhydrase IX: regulation and role in cancer. *Sub-cellular biochemistry* **75**: 199-219.

Birben E, Sahiner UM, Sackesen C, Erzurum S and Kalayci O (2012) Oxidative stress and antioxidant defense. *The World Allergy Organization journal* **5**(1): 9-19.

Chandel NS, McClintock DS, Feliciano CE, Wood TM, Melendez JA, Rodriguez AM and Schumacker PT (2000) Reactive oxygen species generated at mitochondrial complex III stabilize hypoxia-inducible factor-1alpha during hypoxia: a mechanism of O2 sensing. *Journal of Biological Chemistry* **275**(33): 25130-25138.

Chattopadhyay S, Moran RG and Goldman ID (2007) Pemetrexed: biochemical and cellular pharmacology, mechanisms, and clinical applications. *Molecular Cancer Therapeutics* **6**(2): 404-417.

Chen WH, Horoszewicz JS, Leong SS, Shimano T, Penetrante R, Sanders WH, Berjian R, Douglass HO, Martin EW and Chu TM (1982) Human pancreatic adenocarcinoma: in vitro and in vivo morphology of a new tumor line established from ascites. *In Vitro* **18**(1): 24-34.

Clayton DA and Shadel GS (2014) Isolation of mitochondria from tissue culture cells. *Cold Spring Harbor Protocols* **2014**(10): pdb.prot080002.

Dekhne AS, Shah K, Ducker GS, Katinas JM, Wong-Roushar J, Nayeen MJ, Doshi A, Ning C, Bao X, Fruhauf J, Liu J, Wallace-Povirk A, O'Connor C, Dzinic SH, White K, Kushner J, Kim S, Huttemann M, Polin L, Rabinowitz JD, Li J, Hou Z, Dann CE, Gangjee A and Matherly LH (2019) Novel pyrrolo[3,2-d]pyrimidine compounds target mitochondrial and cytosolic one-carbon metabolism with broad-spectrum antitumor efficacy. *Mol Cancer Ther*.

Deng Y, Wang Y, Cherian C, Hou Z, Buck SA, Matherly LH and Gangjee A (2008) Synthesis and Discovery of High Affinity Folate Receptor-Specific Glycinamide Ribonucleotide Formyltransferase Inhibitors With Antitumor Activity. *Journal of Medicinal Chemistry* **51**(16): 5052-5063.

Deng Y, Zhou X, Desmoulin SK, Wu J, Cherian C, Hou Z, Matherly LH and Gangjee A (2009) Synthesis and biological activity of a novel series of 6-substituted thieno[2,3-d]pyrimidine antifolate inhibitors of purine biosynthesis with selectivity for high affinity folate receptors over the reduced folate carrier and proton-coupled folate transporter for cellular entry. *Journal of Medicinal Chemistry* **52**(9): 2940-2951.

Desmoulin SK, Hou Z, Gangjee A and Matherly LH (2012) The human proton-coupled folate transporter: Biology and therapeutic applications to cancer. *Cancer biology & therapy* **13**(14): 1355-1373.

Ducker Gregory S, Chen L, Morscher Raphael J, Ghergurovich Jonathan M, Esposito M, Teng X, Kang Y and Rabinowitz Joshua D (2016) Reversal of cytosolic one-carbon flux compensates for loss of the mitochondrial folate pathway. *Cell Metabolism* **24**(4): 640-641.

Ducker GS, Ghergurovich JM, Mainolfi N, Suri V, Jeong SK, Hsin-Jung Li S, Friedman A, Manfredi MG, Gitai Z, Kim H and Rabinowitz JD (2017) Human SHMT inhibitors reveal defective glycine import as a targetable metabolic vulnerability of diffuse large B-cell lymphoma. *Proceedings of the National Academy of Sciences* **114**(43): 11404-11409.

Ducker GS and Rabinowitz JD (2017) One-Carbon Metabolism in Health and Disease. *Cell Metabolism* **25**(1): 27-42.

Eruslanov E and Kusmartsev S (2010) Identification of ROS Using Oxidized DCFDA and Flow-Cytometry, in *Advanced Protocols in Oxidative Stress II* (Armstrong D ed) pp 57-72, Humana Press, Totowa, NJ.

Flintoff WF, Davidson SV and Siminovitch L (1976) Isolation and partial characterization of three methotrexate-resistant phenotypes from Chinese hamster ovary cells. *Somatic Cell and Molecular Genetics* **2**(3): 245-261.

Gower WR, Jr., Risch RM, Godellas CV and Fabri PJ (1994) HPAC, a new human glucocorticoid-sensitive pancreatic ductal adenocarcinoma cell line. *In Vitro Cell Dev Biol Anim* **30A**(3): 151-161.

Guzy RD, Hoyos B, Robin E, Chen H, Liu L, Mansfield KD, Simon MC, Hammerling U and Schumacker PT (2005) Mitochondrial complex III is required for hypoxia-induced ROS production and cellular oxygen sensing. *Cell Metabolism* **1**(6): 401-408.

Hanahan D and Weinberg Robert A (2011) Hallmarks of Cancer: The Next Generation. *Cell* **144**(5): 646-674.

Hoxhaj G, Hughes-Hallett J, Timson RC, Ilagan E, Yuan M, Asara JM, Ben-Sahra I and Manning BD (2017) The mTORC1 Signaling Network Senses Changes in Cellular Purine Nucleotide Levels. *Cell reports* **21**(5): 1331-1346.

Jain M, Nilsson R, Sharma S, Madhusudhan N, Kitami T, Souza AL, Kafri R, Kirschner MW, Clish CB and Mootha VK (2012) Metabolite Profiling Identifies a Key Role for Glycine in Rapid Cancer Cell Proliferation. *Science (New York, NY)* **336**(6084): 1040-1044.

Kim D, Fiske BP, Birsoy K, Freinkman E, Kami K, Possemato R, Chudnovsky Y, Pacold ME, Chen WW, Cantor JR, Shelton LM, Gui DY, Kwon M, Ramkissoon SH, Ligon KL, Kang SW, Snuderl M, Heiden MGV and Sabatini DM (2015) SHMT2 drives glioma cell survival in the tumor microenvironment but imposes a dependence on glycine clearance. *Nature* **520**(7547): 363-367.

Kolaj-Robin O, O'Kane SR, Nitschke W, Léger C, Baymann F and Soulimane T (2011) Biochemical and biophysical characterization of succinate: Quinone reductase from Thermus thermophilus. *Biochimica et Biophysica Acta (BBA) - Bioenergetics* **1807**(1): 68-79.

Kugel Desmoulin S, Wang L, Hales E, Polin L, White K, Kushner J, Stout M, Hou Z, Cherian C, Gangjee A and Matherly LH (2011) Therapeutic Targeting of a Novel 6-Substituted Pyrrolo [2,3-d]pyrimidine Thienoyl Antifolate to Human Solid Tumors Based on Selective Uptake by the Proton-Coupled Folate Transporter. *Molecular Pharmacology* **80**(6): 1096-1107.

Laemmli UK (1970) Cleavage of structural proteins during the assembly of the head of bacteriophage T4. *Nature* **227**(5259): 680-685.

Lawrence SA, Hackett JC and Moran RG (2011) Tetrahydrofolate Recognition by the Mitochondrial Folate Transporter. *Journal of Biological Chemistry* **286**(36): 31480-31489.

Lawrence SA, Titus SA, Ferguson J, Heineman AL, Taylor SM and Moran RG (2014) Mammalian mitochondrial and cytosolic folylpolyglutamate synthetase maintain the subcellular compartmentalization of folates. *Journal of Biological Chemistry* **289**(42): 29386-29396.

Lee KM, Nguyen C, Ulrich AB, Pour PM and Ouellette MM (2003) Immortalization with telomerase of the Nestin-positive cells of the human pancreas. *Biochem Biophys Res Commun* **301**(4): 1038-1044.

Liang S-Q, Bührer ED, Berezowska S, Marti TM, Xu D, Froment L, Yang H, Hall SRR, Vassella E, Yang Z, Kocher GJ, Amrein MA, Riether C, Ochsenbein AF, Schmid RA and Peng R-W (2018) mTOR mediates a mechanism of resistance to chemotherapy and defines a rational combination strategy to treat KRAS-mutant lung cancer. *Oncogene* **38**(5): 622-636.

Lim HJ, Crowe P and Yang JL (2015) Current clinical regulation of PI3K/PTEN/Akt/mTOR signalling in treatment of human cancer. *Journal of cancer research and clinical oncology* **141**(4): 671-689.

Lin BF, Huang RF and Shane B (1993) Regulation of folate and one-carbon metabolism in mammalian cells. III. Role of mitochondrial folylpoly-gamma-glutamate synthetase. *Journal of Biological Chemistry* **268**(29): 21674-21679.

Loayza-Puch F, Rooijers K, Buil LC, Zijlstra J, Oude Vrielink JF, Lopes R, Ugalde AP, van Breugel P, Hofland I, Wesseling J, van Tellingen O, Bex A and Agami R (2016) Tumour-specific proline vulnerability uncovered by differential ribosome codon reading. *Nature* **530**(7591): 490-494.

Lowry OH, Rosebrough NJ, Farr AL and Randall RJ (1951) Protein measurement with the Folin phenol reagent. *Journal of Biological Chemistry* **193**(1): 265-275.

Lucas S, Chen G, Aras S and Wang J (2018) Serine catabolism is essential to maintain mitochondrial respiration in mammalian cells. *Life Science Alliance* **1**(2): e201800036.

Magnuson B, Ekim B and Fingar DC (2012) Regulation and function of ribosomal protein S6 kinase (S6K) within mTOR signalling networks. *The Biochemical journal* **441**(1): 1-21.

Mann KM, Ying H, Juan J, Jenkins NA and Copeland NG (2016) KRAS-related proteins in pancreatic cancer. *Pharmacology & Therapeutics* **168**: 29-42.

Matherly LH, Hou Z and Deng Y (2007) Human reduced folate carrier: translation of basic biology to cancer etiology and therapy. *Cancer metastasis reviews* **26**(1): 111-128.

Matherly LH, Voss MK, Anderson LA, Fry DW and Goldman ID (1985) Enhanced polyglutamylation of aminopterin relative to methotrexate in the Ehrlich ascites tumor cell in vitro. *Cancer research* **45**(3): 1073-1078.

Matsudaira P (1987) Sequence from picomole quantities of proteins electroblotted onto polyvinylidene difluoride membranes. *Journal of Biological Chemistry* **262**(21): 10035-10038.

McCarthy EA, Titus SA, Taylor SM, Jackson-Cook C and Moran RG (2004) A mutation inactivating the mitochondrial inner membrane folate transporter creates a glycine requirement for survival of chinese hamster cells. *Journal of Biological Chemistry* **279**(32): 33829-33836.

Meiser J, Tumanov S, Maddocks O, Labuschagne CF, Athineos D, Van Den Broek N, Mackay GM, Gottlieb E, Blyth K, Vousden K, Kamphorst JJ and Vazquez A (2016) Serine one-carbon catabolism with formate overflow. *Science advances* **2**(10): e1601273.

Mendoza MC, Er EE and Blenis J (2011) The Ras-ERK and PI3K-mTOR pathways: cross-talk and compensation. *Trends in biochemical sciences* **36**(6): 320-328.

Minton DR, Nam M, McLaughlin DJ, Shin J, Bayraktar EC, Alvarez SW, Sviderskiy VO, Papagiannakopoulos T, Sabatini DM, Birsoy K and Possemato R (2018) Serine Catabolism by SHMT2 Is Required for Proper Mitochondrial Translation Initiation and Maintenance of Formylmethionyl-tRNAs. *Molecular Cell* **69**(4): 610-621.e615.

Mitchell-Ryan S, Wang Y, Raghavan S, Ravindra MP, Hales E, Orr S, Cherian C, Hou Z, Matherly LH and Gangjee A (2013) Discovery of 5-substituted pyrrolo[2,3-d]pyrimidine antifolates as dual acting inhibitors of glycinamide ribonucleotide formyltransferase and 5-aminoimidazole-4-carboxamide ribonucleotide formyltransferase in de novo purine nucleotide biosynthesis: implications of inhibiting 5-aminoimidazole-4-carboxamide ribonucleotide formyltransferase to AMPK activation and anti-tumor activity. *Journal of Medicinal Chemistry* **56**(24): 10016-10032.

Morscher RJ, Ducker GS, Li SH, Mayer JA, Gitai Z, Sperl W and Rabinowitz JD (2018) Mitochondrial translation requires folate-dependent tRNA methylation. *Nature* **554**(7690): 128-132.

Munujos P, Coll-Canti J, Gonzalez-Sastre F and Gella FJ (1993) Assay of succinate dehydrogenase activity by a colorimetric-continuous method using iodonitrotetrazolium chloride as electron acceptor. *Analytical biochemistry* **212**(2): 506-509.

Newman AC and Maddocks ODK (2017) Serine and Functional Metabolites in Cancer. *Trends Cell Biol* **27**(9): 645-657.

Nilsson R, Jain M, Madhusudhan N, Sheppard NG, Strittmatter L, Kampf C, Huang J, Asplund A and Mootha VK (2014) Metabolic enzyme expression highlights a key role for MTHFD2 and the mitochondrial folate pathway in cancer. *Nature communications* **5**: 4128.

Noguchi K, Konno M, Koseki J, Nishida N, Kawamoto K, Yamada D, Asaoka T, Noda T, Wada H, Gotoh K, Sakai D, Kudo T, Satoh T, Eguchi H, Doki Y, Mori M and Ishii H (2018) The mitochondrial one-carbon metabolic pathway is associated with patient survival in pancreatic cancer. *Oncology letters* **16**(2): 1827-1834.

Racanelli AC, Rothbart SB, Heyer CL and Moran RG (2009) Therapeutics by cytotoxic metabolite accumulation: Pemetrexed causes ZMP accumulation, AMPK activation, and mTOR inhibition. *Cancer research* **69**(13): 5467-5474.

Ravindra MP, Wilson MR, Tong N, O'Connor C, Karim MA, Polin L, Wallace-Povirk A, White K, Kushner J, Hou Z, Matherly LH and Gangjee A (2018) Fluorinated Substituted Pyrrolo[2,3-d]Pyrimidine Antifolates With Tumor-Targeting Via Cellular Uptake by Folate Receptor α and the Proton-coupled Folate Transporter and Inhibition of De Novo Purine Nucleotide Biosynthesis. *Journal of Medicinal Chemistry* **61**(9): 4228-4248.

Rosowsky A (1999) PT523 and other aminopterin analogs with a hemiphthaloyl-L-ornithine side chain: exceptionally tight-binding inhibitors of dihydrofolate reductase which are transported by the reduced folate carrier but cannot form polyglutamates. *Current medicinal chemistry* **6**(4): 329-352.

Rothbart SB, Racanelli AC and Moran RG (2010) Pemetrexed indirectly activates the metabolic kinase AMPK in human carcinomas. *Cancer research* **70**(24): 10299-10309.

Royer GP, Ikeda SI and Lee TK (1977) Substrate-induced conformational changes in lactate dehydrogenase. Proteolysis of the immobilized enzyme in the presence of specific substrates. *Journal of Biological Chemistry* **252**(24): 8775-8777.

Schoumacher RA, Ram J, Iannuzzi MC, Bradbury NA, Wallace RW, Hon CT, Kelly DR, Schmid SM, Gelder FB, Rado TA and et al. (1990) A cystic fibrosis pancreatic adenocarcinoma cell line. *Proc Natl Acad Sci U S A* **87**(10): 4012-4016.

Shane B (1989) Folylpolyglutamate synthesis and role in the regulation of one-carbon metabolism. *Vitam Horm* **45**: 263-335.

Stubbs M, McSheehy PMJ, Griffiths JR and Bashford CL (2000) Causes and consequences of tumour acidity and implications for treatment. *Molecular Medicine Today* **6**(1): 15-19.

Subhi AL, Tang B, Balsara BR, Altomare DA, Testa JR, Cooper HS, Hoffman JP, Meropol NJ and Kruger WD (2004) Loss of methylthioadenosine phosphorylase and elevated ornithine decarboxylase is common in pancreatic cancer. *Clin Cancer Res* **10**(21): 7290-7296.

Tan MH, Nowak NJ, Loor R, Ochi H, Sandberg AA, Lopez C, Pickren JW, Berjian R, Douglass HO, Jr. and Chu TM (1986) Characterization of a new primary human pancreatic tumor line. *Cancer Invest* **4**(1): 15-23.

Tibbetts AS and Appling DR (2010) Compartmentalization of Mammalian folate-mediated one-carbon metabolism. *Annual Review of Nutrition* **30**: 57-81.

Unal ES, Zhao R, Qiu A and Goldman ID (2008) N-linked glycosylation and its impact on the electrophoretic mobility and function of the human proton-coupled folate transporter (HsPCFT). *Biochim Biophys Acta* **1778**(6): 1407-1414.

Wang B, Wang W, Zhu Z, Zhang X, Tang F, Wang D, Liu X, Yan X and Zhuang H (2017) Mitochondrial serine hydroxymethyltransferase 2 is a potential diagnostic and prognostic biomarker for human glioma. *Clinical neurology and neurosurgery* **154**: 28-33.

Wang L, Desmoulin SK, Cherian C, Polin L, White K, Kushner J, Fulterer A, Chang M-H, Mitchell S, Stout M, Romero MF, Hou Z, Matherly LH and Gangjee A (2011) Synthesis, biological and antitumor activity of a highly potent 6-substituted pyrrolo[2,3-d]pyrimidine thienoyl antifolate inhibitor with proton-coupled folate transporter and folate receptor selectivity over the reduced folate carrier that inhibits β-glycinamide ribonucleotide formyltransferase. *Journal of Medicinal Chemistry* **54**(20): 7150-7164.

Wang L, Wallace A, Raghavan S, Deis SM, Wilson MR, Yang S, Polin L, White K, Kushner J, Orr S, George C, O'Connor C, Hou Z, Mitchell-Ryan S, Dann CE, Matherly LH and Gangjee A (2015) 6-Substituted Pyrrolo[2,3-d]pyrimidine Thienoyl Regioisomers as Targeted Antifolates for Folate Receptor α and the Proton-Coupled Folate Transporter in Human Tumors. *Journal of medicinal chemistry* **58**(17): 6938-6959.

Wong SC, Proefke SA, Bhushan A and Matherly LH (1995) Isolation of human cDNAs that restore methotrexate sensitivity and reduced folate carrier activity in methotrexate transport-defective Chinese hamster ovary cells. *Journal of Biological Chemistry* **270**(29): 17468-17475.

Wu M, Arimura GK and Yunis AA (1977) Purification and characterization of a plasminogen activator secreted by cultured human pancreatic carcinoma cells. *Biochemistry* **16**(9): 1908-1913.

Wu M, Wanggou S, Li X, Liu Q and Xie Y (2017) Overexpression of mitochondrial serine hydroxyl-methyltransferase 2 is associated with poor prognosis and promotes cell proliferation and invasion in gliomas. *OncoTargets and Therapy* **10**: 3781-3788.

Yang M and Vousden KH (2016) Serine and one-carbon metabolism in cancer. *Nature Reviews Cancer* **16**(10): 650-662.

Ye J, Fan J, Venneti S, Wan YW, Pawel BR, Zhang J, Finley LW, Lu C, Lindsten T, Cross JR, Qing G, Liu Z, Simon MC, Rabinowitz JD and Thompson CB (2014) Serine catabolism regulates mitochondrial redox control during hypoxia. *Cancer discovery* **4**(12): 1406-1417.

Zhang C, Samanta D, Lu H, Bullen JW, Zhang H, Chen I, He X and Semenza GL (2016a) Hypoxia induces the breast cancer stem cell phenotype by HIF-dependent and ALKBH5-mediated m(6)A-demethylation of NANOG mRNA. *Proc Natl Acad Sci U S A* **113**(14): E2047-2056.

Zhang L, Chen Z, Xue D, Zhang Q, Liu X, Luh F, Hong L, Zhang H, Pan F, Liu Y, Chu P, Zheng S, Lou G and Yen Y (2016b) Prognostic and therapeutic value of mitochondrial serine hydroxyl-methyltransferase 2 as a breast cancer biomarker. *Oncology reports* **36**(5): 2489-2500.

Zhao R (2009) A Role for the Proton-coupled Folate Transporter (PCFT-SLC46A1) in Folate. **284**(7): 4267-4274.

Zhao RD-B, Ndeye; Visentin, Michele; Goldman, David I. (2011) Mechanisms of Membrane Transport of Folates into Cells and Across Epithelia. *Annual Review of Nutrition* **31**(1): 177-201.

Zheng Y, Lin TY, Lee G, Paddock MN, Momb J, Cheng Z, Li Q, Fei DL, Stein BD, Ramsamooj S, Zhang G, Blenis J and Cantley LC (2018) Mitochondrial One-Carbon Pathway Supports Cytosolic Folate Integrity in Cancer Cells. *Cell* **175**(6): 1546-1560.e1517.

Footnotes

A.Dekhne and C. Ning contributed equally.

L.H. Matherly and A. Gangjee contributed equally.

Table 1. IC$_{50}$ values for anti-proliferative activities toward HCT116 colon cancer and pancreatic cancer cell line panel							
Compound	**Proliferation Inhibition [IC$_{50}$ (nM)]**						
	HCT116	**MIA PaCa-2**	**HPAC**	**BxPC-3**	**CFPAC**	**AsPC-1**	**HPNE**
AGF291	2121 (1609-2795)	2294 (2110-2493)	309 (268-355)	251 (229-274)	419 (304-578)	284 (261-310)	>5000
AGF320	742 (486-1134)	1540 (1503-1578)	739 (606-901)	632 (425-940)	1912 (1621-2256)	436 (419-453)	>5000
AGF347	347 (301-400)	639 [542-753]	194 (157-239)	80 (72-89)	317 (284-354)	203 (122-337)	>5000

Proliferation inhibition assays were performed using the HCT116 (colon cancer), MIA PaCa-2, HPAC, BxPC-3, CFPAC and AsPC-1 (all PaC), and HPNE (human normal pancreatic epithelial) cell lines. Results are shown as geometric mean IC$_{50}$ values (with 95% confidence interval), corresponding to the concentrations that inhibit growth by 50% relative to vehicle-treated control cells, from three biological replicates.

Table 2: Transport kinetics for 6-substituted pyrrolo[3,2-d]pyrimidine analogs compared to MTX, PMX and AGF94.								
Substrate	**RFC (R1-11 RFC2) pH 7.2**				**PCFT (R2/PCFT4) pH 5.5**			
	K_m (µM)	V_{max} (pmol/mg/min)	V_{max}/K_m	K_i (µM)	K_m (µM)	V_{max} (pmol/mg/min)	V_{max}/K_m	K_i (µM)
MTX	0.609 (0.597-0.622)	80 (44-144)	118 (110-126)	ND	0.329 (0.245-0.441)	404 (184-888)	1230 (687-2204)	ND
PMX	ND	ND	ND	0.583 (0.513-0.663)	ND	ND	ND	0.056 (0.054-0.058)
AGF94	ND	ND	ND	1.614*** (1.423-1.830)	ND	ND	ND	0.070[ns] (0.044-0.111)
AGF291	ND	ND	ND	0.276** (0.225-0.338)	ND	ND	ND	0.163[#] (0.096-0.275)
AGF320	ND	ND	ND	0.200* (0.148-0.272)	ND	ND	ND	0.142* (0.097-0.209)
AGF347	0.388[ns] (0.280-0.536)	72[ns] (68-75)	205 (156-270)	0.247* (0.186-0.327)	0.057* (0.038-0.086)	184 (129-263)	3227 (1499-6945)	0.070*** (0.068-0.073)
Transport assays were performed using engineered R2/PCFT4 (expresses PCFT only) and R1-11 RFC2 (expresses RFC only) cells. For determinations of K_m and V_{max} values by Lineweaver-Burk analysis, concentrations of [³H]**AGF347** or [³H]MTX were from 0.02 to 0.5 µM for R2/PCFT4 (at pH 5.5) and from 0.25 to 5 µM for R1-11 RFC2 (at pH 7.2). K_i values for each of the drugs were determined by Dixon analysis over a range of concentrations of non-radioactive competitor from 0 to 500 nM (for R2/PCFT4 at pH 5.5) or 0 to 1 µM (for R1-11 RFC2 at pH 7.2) and 0.5 µM [³H]MTX. Results are presented as geometric mean values (with 95% confidence intervals) from three biological replicates. Pairwise statistical comparisons were performed against MTX (K_m and V_{max}) and PMX (K_i) using two-sided, unpaired t-test. # denotes $p < 0.1$, * denotes $p < 0.05$, ** denotes $p < 0.01$, and *** denotes $p < 0.001$. ns indicates "no significant difference" when comparing parameters from MTX and **AGF347**. ND, not determined.								

36

Table 3. Subcellular AGF347 metabolite distributions in MIA PaCa-2 cells.		
AGF347 form	**pmol/mg AGF347 metabolite (%)**	
	Cytosol	**Mitochondria**
PG_7	12.87+/-3.52 (6.42%)	36.65+/-4.03 (14.28%)
PG_6	68.03+/-0.37 (33.94%)	115.53+/-6.48 (45.01%)
PG_5	88.30+2.00 (44.05%)	71.26+/-5.17 (27.76%)
PG_4	14.31+/-2.08 (7.41%)	12.59+/2.42 (4.90%)
PG_3	7.45+/-0.76 (3.72%)	8.91+/-1.28 (3.47%)
PG_2	4.50+/-0.40 (2.24%)	4.49+/-1.95 (1.75%)
PG_1 **(AGF347)**	4.00+0.89 (2.49%)	7.52+/-2.43 (2.93%)
Total AGF347 forms	200.45	256.69

MIA PaCa-2 NTC cells were incubated with 2 µM [^{3}H]**AGF347** for 48 h in the presence of adenosine (60 µM) and glycine (130 µM). Cytosolic and mitochondrial cellular fractions were isolated by differential centrifugation and parent (PG_1) and polyglutamyl (PG_2-PG_7) forms were fractionated by reverse phase HPLC and quantified. Results are expressed in units of pmol/mg protein as the average +/- range for biological duplicate experiments and as the percentage of the total **AGF347** forms in each cellular compartment (cytosol and mitochondria)

Figure Legends

Figure 1. C1 metabolism is compartmentalized in the cytosol and the mitochondria. Folates (and folate analogs) enter the cell through plasma membrane folate transporters including PCFT and RFC. Folates then enter the mitochondria by MFT (SLC25A32). Serine catabolism occurs in the mitochondria beginning with SHMT2 to generate glycine and formate. Glycine is used for synthesis of proteins, purines and glutathione (GSH), whereas formate is critical for downstream cytosolic C1 metabolism following formation of 10-formyl-THF. 10-Formyl-THF serves as a C1 donor for the steps catalyzed by GARFTase and AICARFTase in *de novo* purine nucleotide biosynthesis. Formate is also converted to 5,10-methylene (me) THF by 5,10-me-THF dehydrogenase 1 (MTHFD1) which is the cofactor for thymidylate synthase (TS). Arrows indicate the net flux of C1 metabolism but most reactions in the serine/glycine cycle are reversible. Also shown is the SHMT1 reaction in cytosol, which generates serine from glycine and 5,10-me-THF, and the inactivation of ROS by GSH.

Figure 2. *In vitro* antitumor efficacy and identification of targeted pathways and enzymes by **AGF347** in BxPC-3 and HPAC tumor cells by proliferation assays and adenosine/glycine rescue. Dose-response growth inhibition curves are shown for **AGF347** (structure shown) without additions, or in the presence of adenosine (60 µM) and/or glycine (130 µM). The results are mean values +/-standard deviations for three biological replicates.

Figure 3. Plasma membrane uptake of **AGF291**, **AGF320**, and **AGF347**. (A,B) Inhibition of [³H]MTX and [³H]**AGF347** uptake (both at 0.5 µM) in (A) RFC-expressing R1-11 RFC2 HeLa cells at pH 7.2 and (B) PCFT-expressing R2/PCFT4 CHO cells at pH 5.5. **AGF94** and PT523 treatments (both at 10 µM) are used as PCFT- and RFC-specific inhibitor controls, respectively. Results (mean values ± standard deviations) reflect three biological replicates and are expressed

38

as the fraction of [³H]MTX uptake relative to vehicle (i.e. DMSO) treated cells. (C-F) Uptake of

[³H]**AGF347** in HCT116 WT (C) and PaC cells at pH 5.5 (C), pH 7.2 (D), and pH 6.8 (F), without

additions or in the presence of 10 μM **AGF94** and/or PT523. Results (mean values ± standard

deviations) reflect three biological replicates and are expressed as pmol [³H]substrate per mg

protein. #, $p < 0.10$; *, $p < 0.05$; **, $p < 0.01$; ***, $p < 0.001$. "ns" = not significant. Pairwise statistical

comparisons were performed by two-sided unpaired t-tests against R1-11 RFC2 in (A), R2/PCFT4

(B), and none (C-E), unless otherwise specified by lines indicating pairs to be compared.

Experimental details are in **Materials and Methods**.

Figure 4. Subcellular compartmentation of **AGF347** relative to folic acid and MTX. (A-F) Relative

distributions of (A) [³H]folic acid (2.26 μM), (B) [³H]MTX (2 μM), and (C) [³H]**AGF347** (2 μM), as

well as total cellular (D) and compartment-specific accumulations in the cytosol (E) and

mitochondria (F) of glyB (MFT-null) and glyBTII (human MFT transfected) CHO cells and MIA

PaCa-2 NTC (MFT WT) and MIA PaCa-2 MFT KD (MFT KD) PaC cells. Results (mean values ±

standard deviations) represent three biological replicates and are expressed as a percentage (A-

C) or pmol [³H]substrate per mg protein in each cellular fraction (mitochondrial and cytosol) (D-

F). (G-I) HPLC analysis of [³H]**AGF347** polyglutamyl derivatives in the cytosol (G) and

mitochondria (H) of MIA PaCa-2 cells, along with a conjugase-treated aliquot of the cytosol (I).

Results are expressed as counts per minute (CPM) eluted in a given time fraction (see **Materials**

and Methods) and are representative of two biological replicates. #, $p < 0.10$; *, $p < 0.05$; **, $p <$

0.01; ***, $p < 0.001$. "ns" = not significant. Pairwise statistical comparisons were performed by

two-sided unpaired t-tests and each line indicates a pair to be compared in (panels D-F).

Figure 5. Inhibition of mTOR signaling by **AGF291**, **AGF320**, and **AGF347**. (A,B) Activation of

AMPK and suppression of mTOR signaling via S6K1 (mTOR effector, p85 and p70 isoforms) in

vehicle-, AICAR-, or drug-treated KRAS WT BxPC-3 and KRAS mutant HPAC cells. The cell lines

were analyzed on the same gel with a single marker. AMPK activation is reflected in the hyperphosphorylation (P-AMPK) and S6K1 suppression is reflected in the hypophosphorylation of p85-S6K1 and p70-S6K1 (P-p85-S6K1 and P-p70-S6K1). Total AMPK and p85-S6K1 and p70-S6K1 are shown. β-Actin was used as a loading control. Blots are representative of three biological replicates. Experimental details are in **Materials and Methods**.

Figure 6. Effects of **AGF347** on mitochondrial respiration. Oxygen consumption rate (OCR) measurements of vehicle-treated HCT116 WT or SHMT2 KO cells, and of **AGF347**-treated HCT116 WT cells during a mitochondrial stress test are shown. Experiments were performed with a Seahorse XeF-24 analyzer with HCT116 cells pretreated with vehicle (DMSO; WT and SHMT2 KO) or 10 μM **AGF347** (WT) for 48 h in glycine-replete media with 60 μM adenosine. Oligomycin (1 μM), FCCP (1 μM), and rotenone/antimycin A (1 μM each) were sequentially added at the indicated time points to determine basal, maximal, and non-mitochondrial respiration, as well as H^+ leak. Results (mean values ± standard errors) represent 12 technical replicates measured over two independent experiments. #, $p < 0.10$; *, $p < 0.05$; **, $p < 0.01$; ***, $p < 0.001$. "ns" = not significant. Pairwise statistical comparisons were performed by two-sided unpaired t-tests against WT. Experimental details are in **Materials and Methods**.

Figure 7. Effects of **AGF347** on ROS and reduced (GSH) and total (GSH + GSSG) glutathione pools. (A) Carbonic anhydrase IX (CA9) transcripts were measured as a biological readout for hypoxia in HCT116 (WT, SHMT1 KO, and SHMT2 KO) and PaC (BxPC-3, HPAC, and MIA PaCa-2) cells incubated for 24 h under normoxic (21% O_2, 5% CO_2) or hypoxic (0.5% O_2, 5% CO_2) conditions. (B,C) Data are shown for cellular ROS generation in vehicle- or **AGF347**-treated cells under normoxia (B) or hypoxia (C). (D) Data are shown for reduced glutathione (GSH) and total glutathione (GSH+GSSG) in vehicle- or **AGF347**-treated cells under hypoxic conditions. CA9 experiments reflect three biological replicates, GSH/GSSG experiments reflect 8 technical

40

replicates over two independent experiments, and ROS experiments represent 16 technical

replicates over two independent experiments. GSH/GSSG and ROS results (mean values ±

standard deviations) were normalized to cellular proteins. #, $p < 0.10$; *, $p < 0.05$; **, $p < 0.01$; ***,

$p < 0.001$. "ns" = not significant. Pairwise statistical comparisons were performed by two-sided

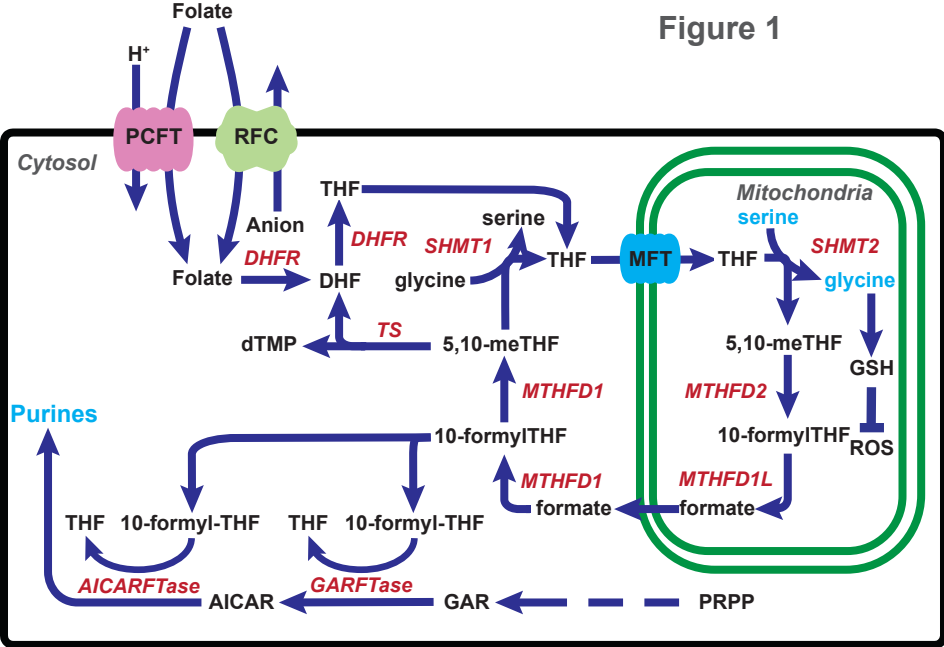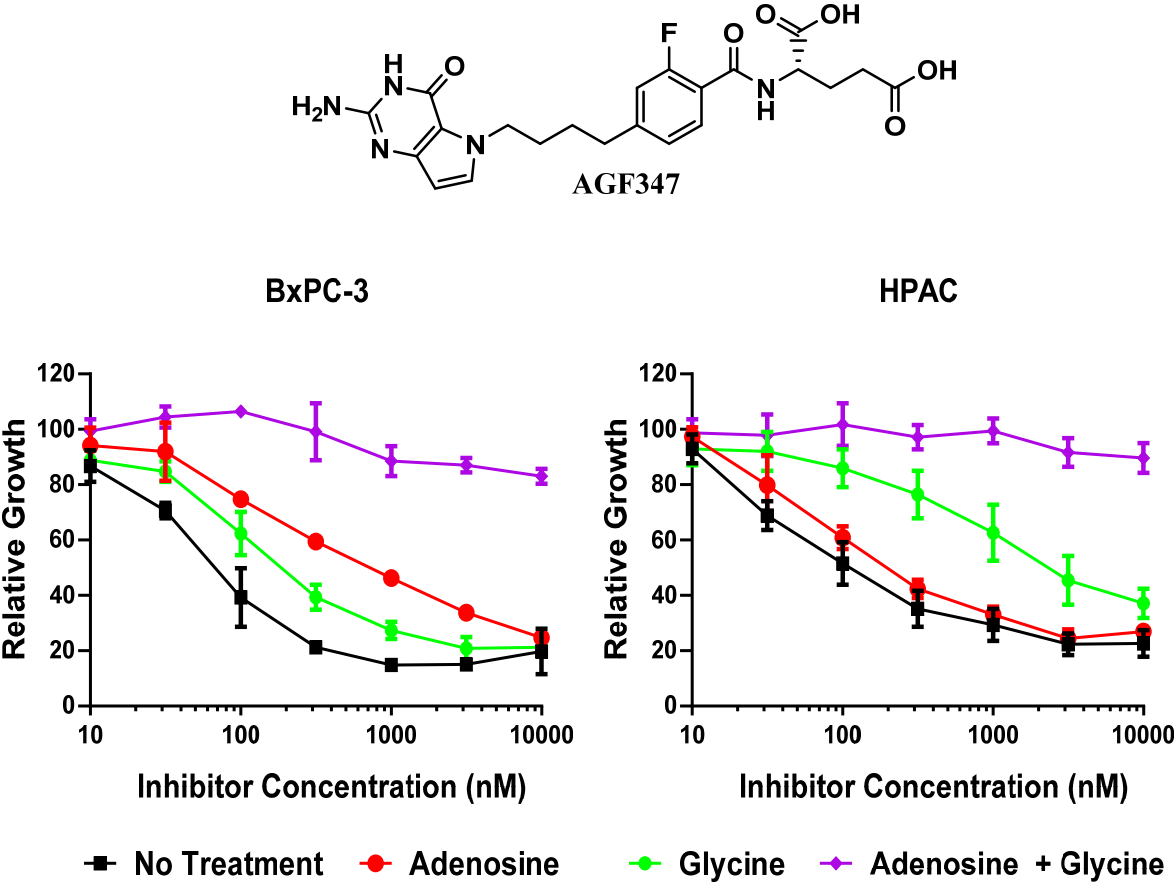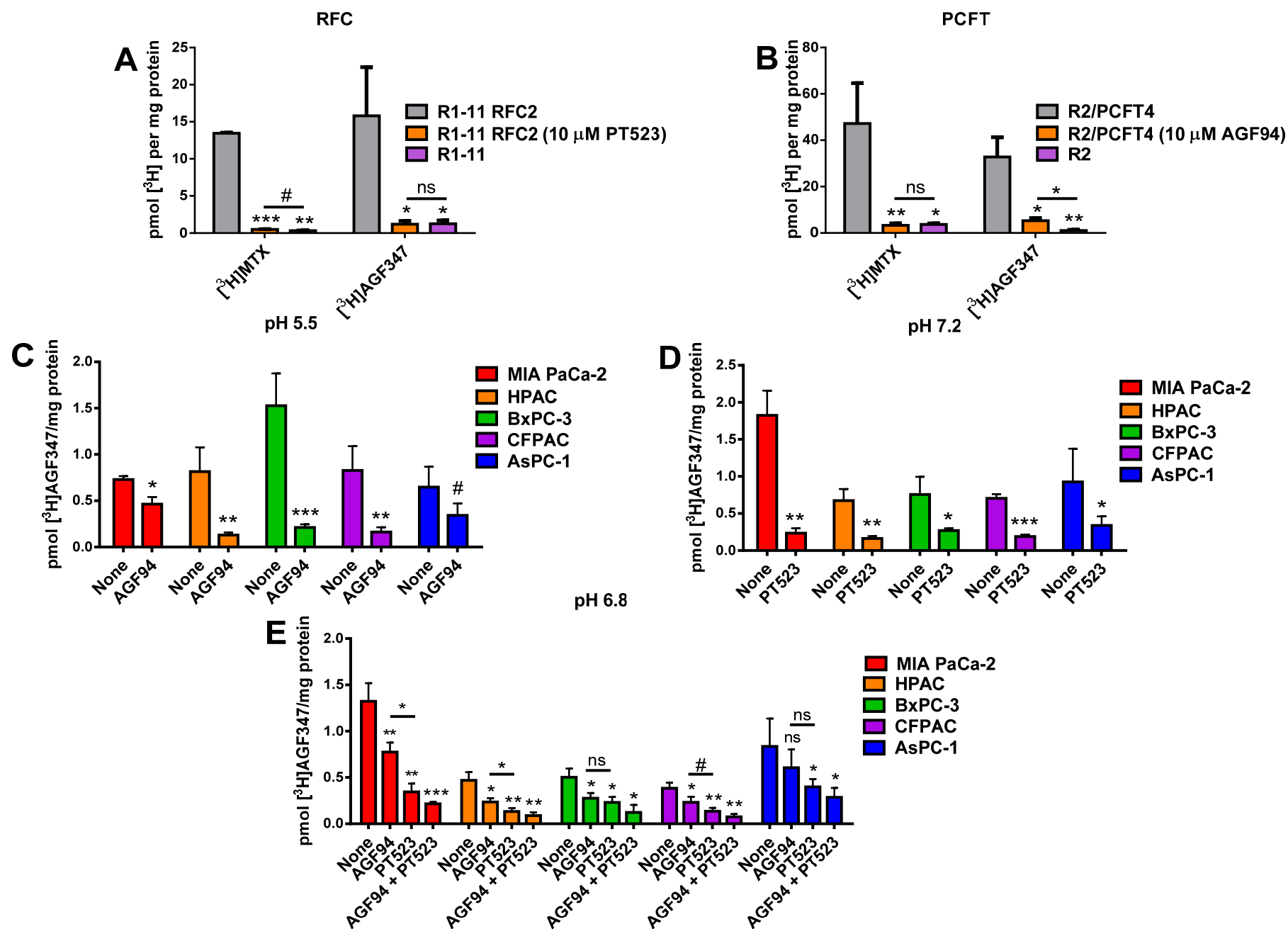unpaired t-tests against normoxia samples in panel A and respective WTs in panels B-D.

Figure 1

Figure 2

AGF347

BxPC-3

HPAC

■ No Treatment ● Adenosine ● Glycine ◆ Adenosine + Glycine
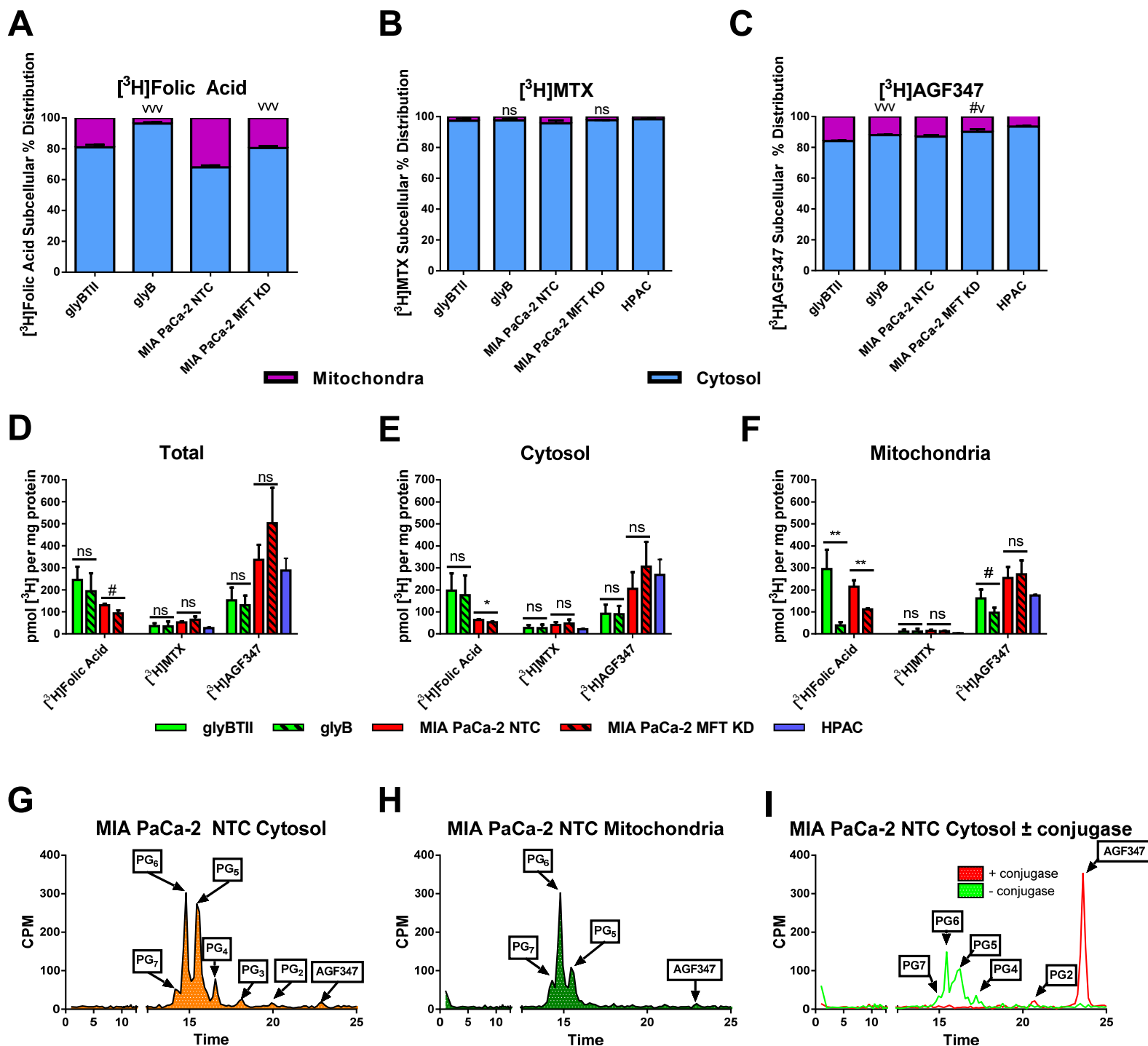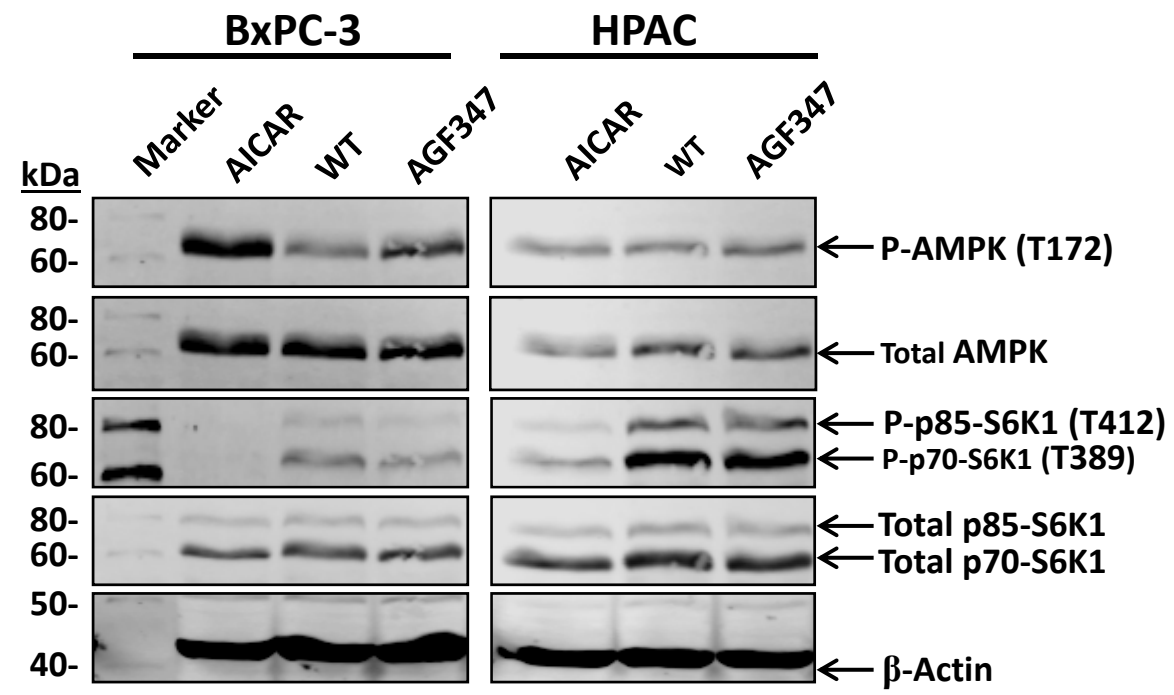
Figure 3

Figure 4

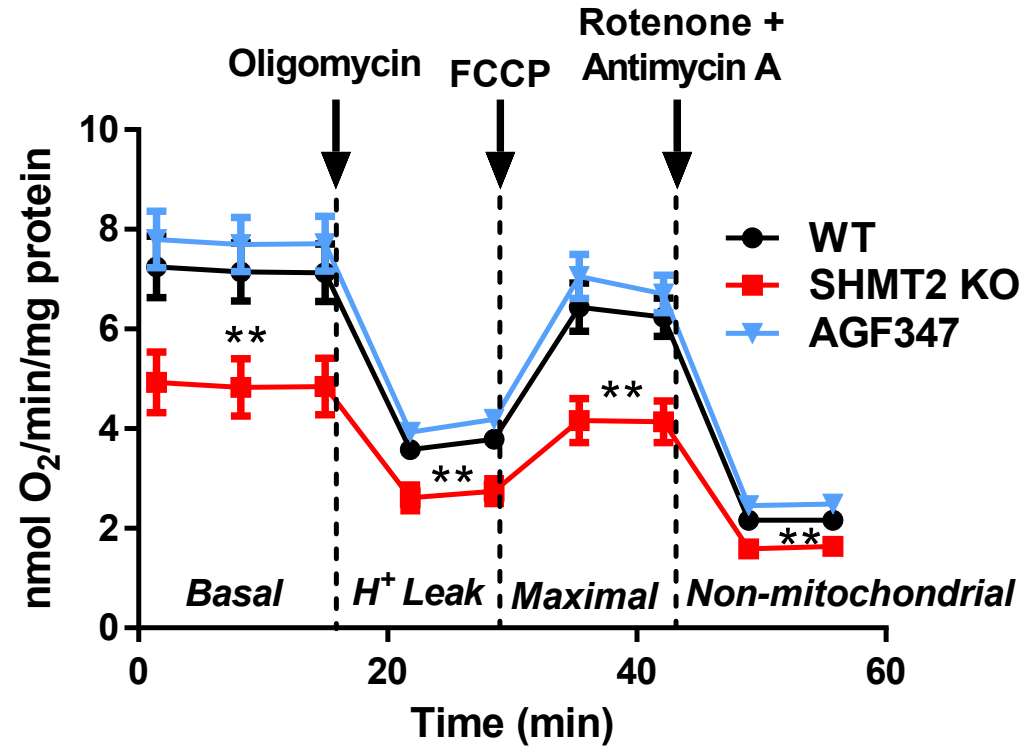# Figure 5
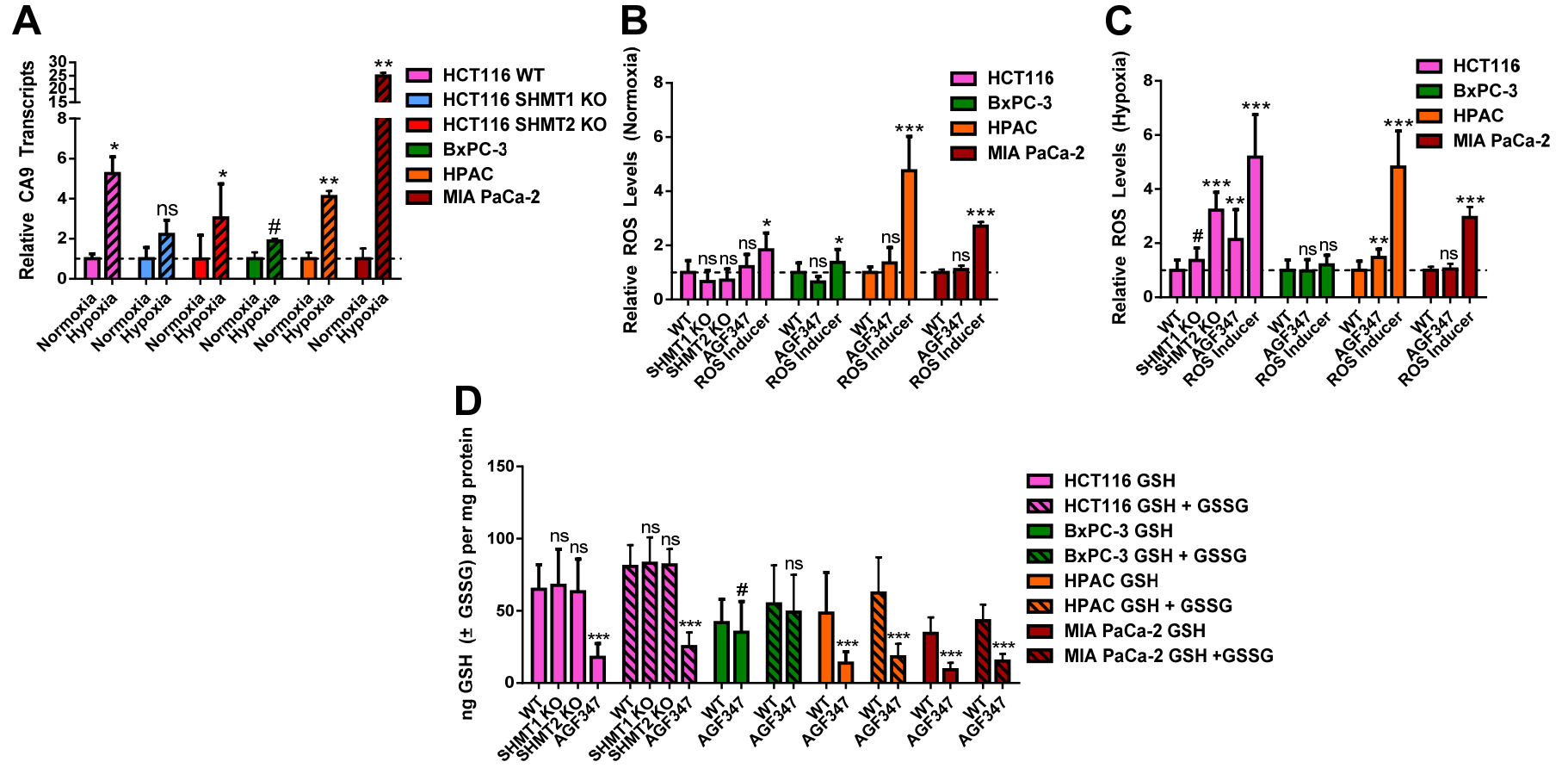
Figure 6

Figure 7

Supplementary Data

Cellular pharmacodynamics of a novel pyrrolo[3,2-*d*]pyrimidine inhibitor targeting

mitochondrial and cytosolic one-carbon metabolism

Aamod S. Dekhne[1], Changwen Ning[4], Md. Junayed Nayeen[2], Khushbu Shah[2], Hasini Kalpage[3], Josephine Frühauf[1], Adrianne Wallace-Povirk[1], Carrie O'Connor[1], Zhanjun Hou[1,5], Seongho Kim[1,5], Maik Hüttemann[3,5], Aleem Gangjee[2]*, and Larry H. Matherly[1,5,6]*

[1]Department of Oncology, Wayne State University School of Medicine / Karmanos Cancer Institute, Detroit, MI 48201

[2]Division of Medicinal Chemistry, Graduate School of Pharmaceutical Sciences, Duquesne University, Pittsburgh, PA 15282

[3]Center for Molecular Medicine and Genetics, Wayne State University School of Medicine, Detroit, MI 48201

[4]Biochemistry and Molecular Biology, Jilin University, Changchun, Jilin Province, China

[5]Molecular Therapeutics Program, Barbara Ann Karmanos Cancer Institute, Detroit, MI 48201

[6]Department of Pharmacology, Wayne State University School of Medicine, Detroit, MI 48201

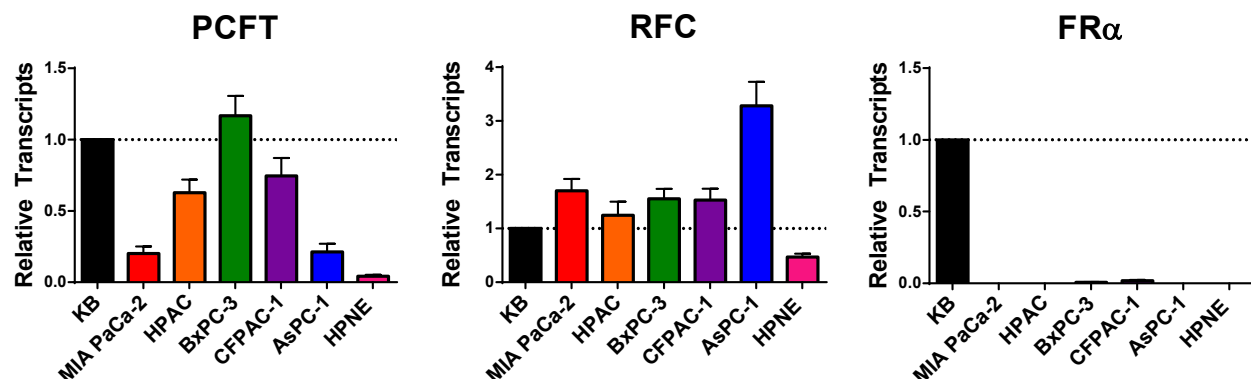*To whom correspondence should be addressed

Figure S1. Relative transcripts of the proton-coupled folate transporter (PCFT), reduced folate carrier (RFC), and folate receptor α (FRα) were measured by RT-PCR in PaC cell lines and HPNE (human pancreatic normal epithelial) cells and compared to those in KB cells, which were assigned a value of 1. Results reflect mean values ± standard deviations of 3 biological replicates with transcript levels for target genes normalized to those of glyceraldehyde-3-phosphate dehydrogenase (GAPDH).
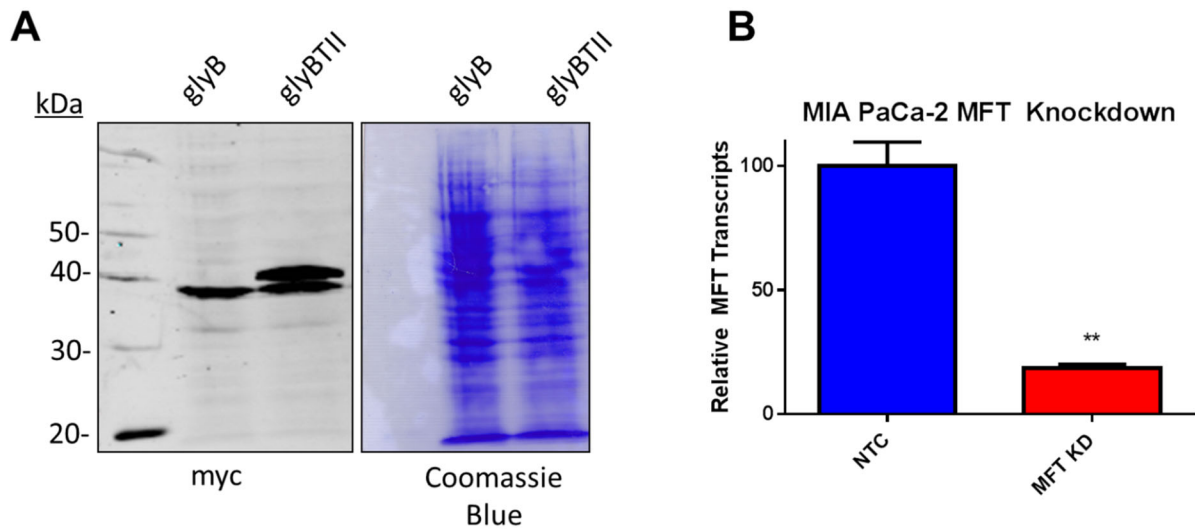
Figure S2. Generation of glyBTII and MIA PaCa-2 MFT KD cell lines. (A) Myc-tagged human MFT cDNA was transfected into glyB cells to generate glyBTII cells. Western Blot of mitochondrial fraction (see **Materials and Methods**) of glyB and glyBTII cells (left) with Coomassie Blue stain of the membrane used as a loading control (right). (B) Relative transcripts of MFT in MIA PaCa-2 cells transduced with non-targeted control (NTC) and MFT-targeted shRNA. Results (mean values ± standard deviations) represent three biological replicates. A pairwise statistical comparison was performed by a two-sided unpaired t-test against NTC. **, p < 0.01.

Table S1: Purity of Subcellular Fractions		
MIA PaCa-2 NTC	**Cytosol**	**Mitochondria**
LDH Activity	96.92 (1.69)	3.08 (1.69)
SDH Activity	77.53 (6.06)	22.47 (6.06)
MIA PaCa-2 MFT KD	**Cytosol**	**Mitochondria**
LDH Activity	97.22 (0.49)	2.78 (0.49)
SDH Activity	83.78 (3.63)	16.22 (3.63)
GlyB	**Cytosol**	**Mitochondria**
LDH Activity	99.62 (0.06)	0.38 (0.06)
SDH Activity	76.94 (10.93)	23.07 (10.93)
GlyBTII	**Cytosol**	**Mitochondria**
LDH Activity	98.48 (2.15)	1.52 (2.15)
SDH Activity	78.04 (2.64)	21.96 (2.64)
HPAC	**Cytosol**	**Mitochondria**
LDH Activity	94.27 (1.51)	5.73 (1.51)
SDH Activity	84.46 (2.07)	15.54 (2.07)

Subcellular fractions were generated as described in the **Materials and Methods**. Lactate dehydrogenase (LDH) and succinate dehydrogenase (SDH) were assayed spectrophotometrically as markers for cytosol and mitochondria respectively. Results reflect three biological replicates and the percentage of total enzyme activity in each fraction (mean ± standard deviation) is provided.